High Temperature Corrosion and Descaling

Camilla Bonvicini



LUND UNIVERSITY

LTH

FACULTY OF ENGINEERING

Master Thesis

Course – MMTM05 Degree Project in Production and Materials engineering

Author: Camilla Bonvicini

Examiner: Filip Lenrick, Docent
Division of Production and Materials Engineering
Department of Industrial and Mechanical Sciences
Faculty of Engineering, Lund University

Supervisors: Jesús Carrero Robles, PhD Candidate
Department of Industrial and Mechanical Sciences
Faculty of Engineering, Lund University

Mehdi Roozban
R&D Materials and Technology Department,
Alfa Laval AB, Sweden

Hector Pous Romero
R&D Materials and Technology Department,
Alfa Laval AB, Sweden

Keywords: austenitic stainless steel, oxidation kinetic, oxide layer, descaling process, acid solution

Acknowledgment

First of all, I would like to thank Lund University, and more specifically the Division of Production and Materials Engineering, for allowing me to experience these two beautiful years full of learning and challenges.

A big thanks to my company supervisors, Mehdi Roozban and Hector Pous Romero. I truly appreciate your help and guidance throughout the five-month journey that was my thesis.

I also want to thank my university supervisor, Jesús Carrero Robles, whose feedback and insights were invaluable in developing the report you are about to read.

Special thanks to Alfa Laval for giving me the opportunity to undertake this thesis and to all the people from the MT&C department: you were always supportive of this research and genuinely kind. I've learned a lot from this experience and I look forward to applying this knowledge in my future work.

Abstract

High temperature corrosion presents a challenge both in predicting material loss over time and in cleaning and reusing the material after oxidation cycles.
This thesis investigates the oxidation behavior and descaling of different austenitic stainless steels exposed to a range of temperatures in an oxygen-rich environment.

The first part of the project focused on developing a descaling method. Two solutions were tested: one containing rock salt and nitric acid, and the other composed of nitric acid and hydrofluoric acid. The second solution was found to be more effective. The resulting samples were examined using both stereoscopic and optical microscopy in order to characterize the surface and cross-sections. The images highlighted a tendency for the descaled samples to exhibit intergranular corrosion or surface erosion, especially after treatment with the rock salt solution. Additionally, it was observed that 950°C was the most critical temperature, producing the worst results in term of descaling.

In the second part of the project, the previously developed descaling method was applied to a selected group of austenitic stainless steels: 304, 310S, 316L and 347. These materials were oxidized for almost 2000 hours at two different service temperatures: 600°C and 800°C. This allowed the development of thickness loss models over time for the tested materials, based on oxidation kinetics.

Among the materials studied, 310S displayed the best performance over time at both temperatures, exhibiting a logarithmic thickness loss behavior. According to the oxidation kinetics, this is the optimal output, as it results in less material loss over time compared to parabolic and linear rates. 347 was found to be the second-best material, also displaying a logarithmic behavior at 800°C. 304 performed well at 600°C but poorly at 800°C, in terms of thickness loss. 316L performed the worst overall, exhibiting a parabolic rate in both cases.

Contents

1 Introduction **7**
- 1.1 Background . . . 7
- 1.2 Aims and Objectives . . . 8
  - 1.2.1 Limitations . . . 9

2 Literature review **10**
- 2.1 Overview of stainless steel . . . 10
  - 2.1.1 Austenitic Stainless steel . . . 11
  - 2.1.2 Sensitization . . . 12
  - 2.1.3 Overview of the austenitic stainless steel used . . . 12
- 2.2 High Temperature Oxidation . . . 13
  - 2.2.1 Oxide film in austenitic stainless steels . . . 15
  - 2.2.2 Chromium depletion layer (CDL) . . . 16
- 2.3 Descaling Method . . . 17
  - 2.3.1 Chemical descaling and pickling . . . 17
  - 2.3.2 Mechanical Descaling . . . 18

3 Methodology **19**
- 3.1 Sample preparation . . . 20
- 3.2 The furnaces . . . 21
- 3.3 Descaling Process . . . 22
- 3.4 Sample preparation: cross section and mounting . . . 25

4 Results and Discussion **27**
- 4.1 Descaling behavior: time observation . . . 27
- 4.2 Mass measurement . . . 28
- 4.3 Stereoscopic microscope analysis . . . 33
- 4.4 Optical microscope analysis . . . 37
  - 4.4.1 Cross section AISI 304 . . . 38
  - 4.4.2 Cross section AISI 310S . . . 41
  - 4.4.3 Cross section AISI 316L . . . 44
  - 4.4.4 Cross section AISI 347 . . . 47
- 4.5 Oxidation Kinetic Models . . . 51

5 Conclusion **54**

6 Future work **55**

List of Figures

1.1 Stainless steel price trends: gap between demand and supply in different markets [10]. 8

2.1 Cr and Ni content in different Stainless Steel alloys [15]. 11
2.2 schematic representation of the oxide layer as a ionic and electronic conductor [34]. . 13
2.3 Ellingham graph, showing the energy of formation of different oxides [34]. 14
2.4 Graphic representation of three oxidation kinetic laws [34]. 15
2.5 Variation of the oxide layer formed at 1000 C based on the amount of chromium [34]. 16
2.6 Overview of different descaling methods [37]. 17

3.1 304 sample on the precision scale after extraction from the oxidation furnace. 20
3.2 Furnaces used in the experimental phases. 21
3.3 Muffle Furnace used during Phase 2. 22
3.4 EFF furnace loaded during Phase 2. 22
3.5 Starting of the descaling process Phase 1. 23
3.6 Color difference in Solution A due to the different stages the sample are in the descaling process. 24
3.7 Starting station for the descaling process in Phase 2. 24
3.8 Samples in different descaling stages during Phase 2. 25
3.9 Mounted samples in the epoxy resin. 26

4.1 Representation of the different descaling times, depending on base material, oxidation temperature and descaling solutions. Green and blue bars represent the different solutions A and B, respectively. 28
4.2 Mass gained per area over time at an oxidation temperature of 800 °C. 30
4.3 Mass gained per area over time at an oxidation temperature of 600 °C. 30
4.4 316L sample before descaling process showing an inhomogeneous oxide layer. 31
4.5 316L comparison weight gained over area at an oxidation temperature of 600°C. . . 32
4.6 310S comparison weight gained over area at an oxidation temperature of 600°C. . . 32
4.7 Stereoscopic images of 304 samples oxidized at different temperatures and descaled using both Solution A (left) vs. Solution B (right). 34
4.8 Stereoscopic images of 310S samples oxidized at different temperatures and descaled using both Solution A (left) vs. Solution B (right). 35
4.9 Stereoscopic images of 316L samples oxidized at different temperatures and descaled using both Solution A (left) vs. Solution B (right). 36
4.10 Stereoscopic images of 347 samples oxidized at different temperatures and descaled using both Solution A (left) vs. Solution B (right). 37
4.11 Time-Temperature Sensitization (TTS) for AISI 304 [47]. 38
4.12 Optical microscope images of cross-sections of 304 samples oxidized at different temperatures. 39

4.13 Optical microscope images of cross-sections of 304 samples oxidized at different temperatures and descaled using Solution A. 40
4.14 Optical microscope images of cross-sections of 304 samples oxidized at different temperatures and descaled using Solution B. 41
4.15 Optical microscope images of cross-sections of 310S samples oxidized at different temperatures. 42
4.16 Optical microscope images of cross-sections of 310S samples oxidized at different temperatures and descaled using Solution A. 43
4.17 Optical microscope images of cross-sections of 310S samples oxidized at different temperatures and descaled using Solution B. 44
4.18 Optical microscope images of cross-sections of 316L samples oxidized at different temperatures. 45
4.19 Optical microscope images of cross-sections of 316L samples oxidized at different temperatures and descaled with Solution A. 46
4.20 Optical microscope images of cross-sections of 316L samples oxidized at different temperatures and descaled with Solution B. 47
4.21 Optical microscope images of cross-sections of 347 samples oxidized at different temperatures. 48
4.22 Optical microscope images of cross-sections of 347 samples oxidized at different temperatures and descaled using Solution A. 49
4.23 Optical microscope images of cross-sections of 347 samples oxidized at different temperatures and descaled using Solution B. 50
4.24 Thickness loss over time - oxidation temperature 800 °C. 51
4.25 Thickness loss over time - oxidation temperature 600 °C. 52

List of Tables

2.1 Composition of the Austenitic Stainless Steel used in the experimental phase (weight %). 13

3.1 Parameters and Materials used in Phase 1 and Phase 2. 19

4.1 Results from the data collected with the stereoscopic microscope. The ✗ symbol indicates that the descaling process was not successful. The ✓ symbol represents that the descaling process was successful. 34

Chapter 1

Introduction

1.1 Background

Corrosion, and more specifically high temperature corrosion, continues to represent a challenge in the service life and maintenance of many of Alfa Laval's products. As leader in the heat exchanger market, this represents issues both in performance and reliability. High-temperature corrosion is defined as a complex degradation process that occurs when a metallic material is exposed to elevated temperatures in environment oxygen-rich for extended periods. Usually, temperatures between 500°C and 1100°C are considered high for theses type of applications [1]. The results of this process varies depending on the material composition, the duration of exposure, the properties of the protective film, and the surrounding environment [2].

Hot corrosion is a specific form of high-temperature corrosion that arises when metallic materials are exposed to sulfate-rich and/or oxide-rich environment at elevated temperatures [3]. This report will focus exclusively on austenitic stainless steel, as Alfa Laval's main products, such as heat exchangers, are made from this specific type of material.

Hot corrosion in stainless steel occurs due to the degradation of the protective chromium oxide. This phenomenon usually proceeds through the following mechanism: initially, oxygen absorption increases rapidly as elevated temperatures facilitate the diffusion of oxygen into the steel surface, creating an oxide film that is supposed to protect the surface from degradation. Over time, the oxide layer thickens. After a prolonged period, which depends on several factors such as temperature and metal composition, the protective film begins to degrade and crack due to both external and internal stresses. This phase is called oxide spallation. The areas where the base material is exposed to the environment due to spallation will form a new oxide layer, increasing chromium depletion [4, 5, 6, 7]. Heat exchangers are particularly vulnerable to hot corrosion, which significantly impacts their performance, especially during extended operation.

In addition, based on the 2025 report, as shown in Figure 1.1, the global stainless steel supply chain is in deficit, as it is incapable of providing the necessary quantities to meet the demand [8]. This deficit is primarily due to the imbalance between production costs and selling prices, which reduces profit margins for producers. In fact, the Nickel pig Iron, which represents the cost-effective alternative of pure Nickel, continues to decrease in price, while production costs remain stable [9]. Moreover, unlike aluminum, stainless steel scrap is more complex and expensive to recycle. Achieving the same quality as virgin material requires more sophisticated and costly processes,

especially to reach the original properties [8]. In this market contest, the ability to reintroduce the stainless steel into the supply chain after descaling will become consistently more important and relevant to reduce shortages and support industry sustainability.

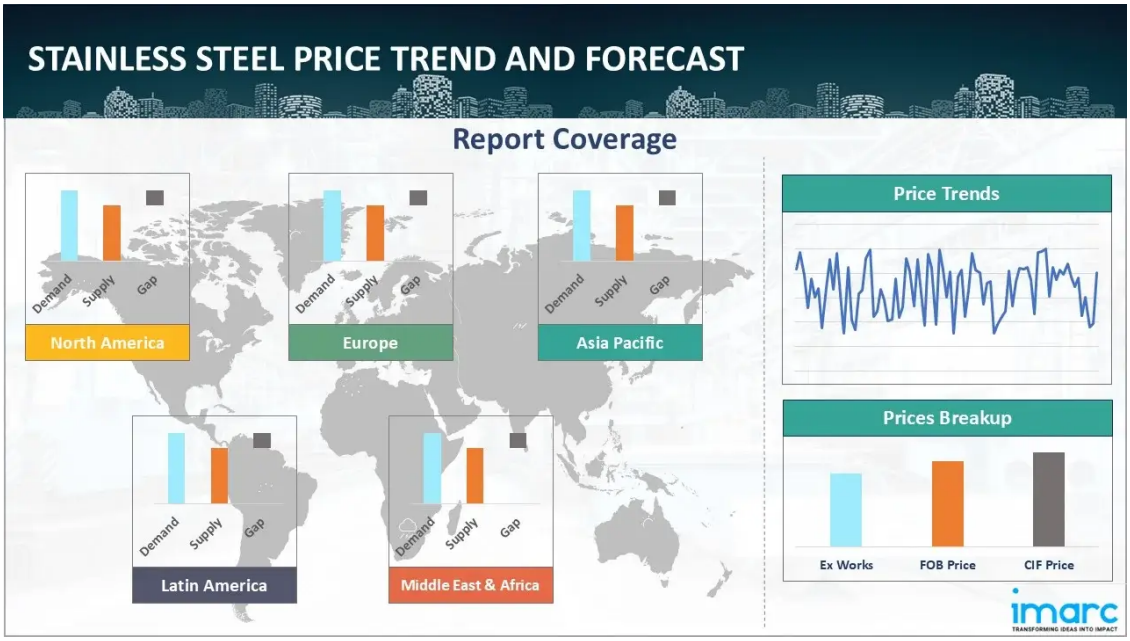


Figure 1.1: Stainless steel price trends: gap between demand and supply in different markets [10].

Given these challenges, this thesis will address how high-temperature corrosion affects various stainless steels at different temperatures and will explore effective methods for removing the resulting oxide layer through both chemical and mechanical descaling processes. This approach will make it possible to investigate the weight loss of different stainless steel materials at specific temperatures, in order to predict material loss over prolonged periods.

1.2 Aims and Objectives

This thesis aims to identify a descaling method that can be effectively applied to various oxidized austenitic stainless steels that have undergone different service temperatures. The method should allow for a simple and efficient process within a reasonable time frame, without causing significant damage of the base material. Additionally, it intends to establish a thickness loss model based on the oxidation kinetics of the descaled alloys, in order to predict the thickness reduction at a specific service temperature.

The objective of this thesis are:

1. To oxidize different stainless steel samples at various service temperatures.
2. To descale the samples with two different acid solutions in order to determine the most efficient method.
3. To characterize the extent of oxide scales and evaluate the efficacy of descaling solutions using optical microscopy.

4. To measure the mass of both the oxidized and descaled samples in order to develop the oxidation kinetic model.

1.2.1 Limitations

The main limitations presented in this dissertation are related to time constraints. To obtain comprehensive and accurate data, multiple samples need to be analyzed. However, three samples per data point will only be considered. Additionally, due to the length of the exposure times required for each test, this study will focus mainly on the temperature of 800°C, which is representative of the most severe operating conditions encountered in Alfa Laval's heat exchangers.

Some tests will also be conducted at 600°C. However, due to spatial constraints in the furnace, a smaller group of samples will be analyzed at this temperature, resulting in fewer data points. This may affect the accuracy of the curve.

Moreover, due to time constraints, only four out of the six initial materials used to study the descaling process will be used to obtain the material loss model. The extent of the samples analysis using optical microscope and SEM will also be limited due to time constraint.

Chapter 2

Literature review

Effective descaling methods for stainless steel capable of removing oxide layers within a reasonable time frame, typically not exceeding six hours and at room temperature, are increasing interest in industry. Avoiding the need to heat acid mixtures reduces the risks associated with hazardous fumes, especially at elevated temperatures (between 50°C and 77°C) [11], and enhances process safety. Moreover, cleaning the material's surface without damaging the matrix is environmentally sustainable as it reduces waste and preserves the integrity of the material. However, the literature on room-temperature descaling method is limited and often focuses on specific materials paired with tailored acid formulations.

As it will be shown in this report, descaling methods can be used to remove the oxide scale and provide important data on material loss. Even when effective, these methods usually result in a minor loss of base material. This material loss can be quantified and used to predict material degradation during specific operating conditions, such as temperature, for that given material. This predictive data is useful for engineers and designers, allowing them to account for material loss during product development phase and specify appropriate material thickness, guaranteeing product reliability and longevity.

The definition of "high temperature" is not universal, as it varies depending on the type of material and its melting point. Therefore, defying what constitutes high temperature is, to some extent, an arbitrary decision. Since the main materials discussed in this report are austenitic stainless steels, "high temperature" will be defined as any temperature above 500 °C. If a different threshold for "high temperature" is necessary for a specific application, it will be explicitly stated. [12].

2.1 Overview of stainless steel

Stainless steel represents one of the most widely used groups of metal globally, thanks to their exceptional corrosion resistance, especially at low temperature. The name "stainless" refers to the material's ability to resist rust, making them ideal for a variety of applications in completely different fields. Even at elevated temperatures, stainless steel remains a common choice due to its durability combined with competitive prices. Stainless steel is usually divided into five main categories: Ferritic stainless steel, Austenitic stainless steel, Martensitic Stainless steel, Precipitation Hardening stainless steel and Duplex Stainless steel. This is shown in Figure 2.1, which exhibits the difference in nickel and chromium content in the five categories. [13, 14].

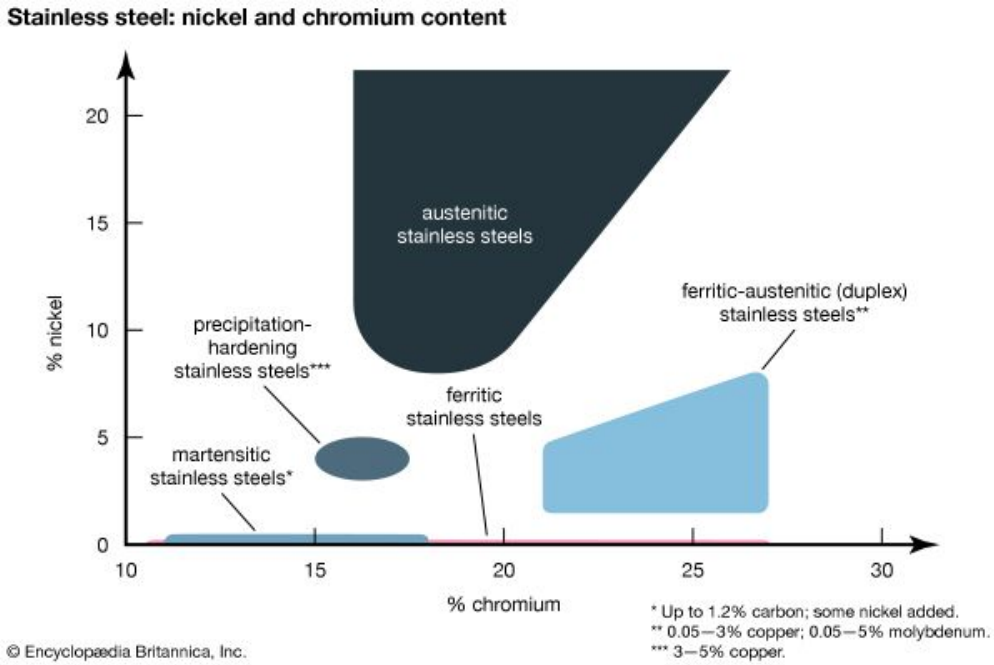


Figure 2.1: Cr and Ni content in different Stainless Steel alloys [15].

2.1.1 Austenitic Stainless steel

Austenitic stainless steel is the most popular and widely used family within the stainless steel group, due to its excellent corrosion resistance in every environment and its diverse mechanical properties. The name "austenite" comes from the resultant phase after solidification: austenite, which has a face centered cubic (FFC) crystal structure. Austenitic stainless steel usually contains between 16-26 wt% chromium and between 8-35 wt% nickel [13, 14].

The alloying elements in the chemical composition play a crucial role both in mechanical properties and corrosion resistance. A brief overview of the main alloying elements and their effects is provided below.

The high Chromium content, as in all stainless steel, provides corrosion resistance by creating a passivation layer. In austenitic stainless steels, the chromium content by weight is typically about 16-26 wt%. Although increasing the chromium content generally improves corrosion resistance, excessive chromium (over the content limit of 26 wt%) can negatively affect other mechanical properties of the steel, such as the weldability. Therefore, it is often more convenient to add more elements to the alloy [13, 14, 16].

Nickel is fundamental for stabilizing the austenite phase during cooling, preventing the formation of martensite, and increasing mechanical properties. Moreover, nickel improves the re-passivation of the chromium oxide layer in different environments. Even though the passivation layer has a self-healing mechanism, nickel increases its resistance, especially in non-oxidizing environment. Additionally, it increases the material's resistance to corrosion, especially against certain mineral acids [13, 14, 16, 17].

Other elements such as titanium, niobium and manganese, can also be found in the chemical composition of stainless steel. Manganese can partially substitute for nickel in the 2xx series,

although this substitution can affect the alloy's formability. Niobium and Titanium are added as stabilizers, they help prevent the formation of chromium carbides, thereby protecting the alloy from intergranular corrosion due to sensitization. Nitrogen is another important element, as it enhances the resistance to pitting corrosion and improves strength, and helps prevent the formation of the sigma σ phase [13, 14]. Molybdenum is also commonly present, as it acts as a stabilizer for the passive film and further improves resistance to corrosion [16]. Another fundamental element present in all austenitic stainless steel is silicon, as it helps prevent the formation of pores between the oxide scale and the matrix [18].

2.1.2 Sensitization

Sensitization is an important phenomenon that affects austenitic stainless steel at high temperatures and can lead to corrosion. When the material is exposed to temperatures between 550°C and 850°C, chromium carbides $Cr_{26}C_6$ tend to precipitate at the grain boundaries. This precipitation depletes chromium in these regions, making the grain boundaries more susceptible to corrosion [19]. The only effective method to correct sensitized stainless steel is annealing. However, each material and composition requires different times, temperatures, and quenching procedures [20].

2.1.3 Overview of the austenitic stainless steel used

- 304 is one of the most versatile metals in the austenitic stainless steel family, representing the perfect balance between performance and cost. Its good corrosion resistance and excellent workability make it suitable for a wide range of applications [21].
- AISI 316L is similar in composition to 304, but contains less carbon. Unlike 304, it also includes molybdenum, which makes it more resistant to corrosion in critical environments, although it is slightly more expensive overall. 304 and 316 are the most widely used metals within the austenitic stainless steel family [21].
- 310S, thanks to its chemical composition with a high level of chromium, the highest in the austenite family, and significant Nickel content, is suitable for high temperature applications, especially over extended periods. However, it is more expensive than a lower grade metal [22].
- 347 is typically chosen for its high resistance to intergranular corrosion, achieved by the presence of stabilizing niobium, which helps avoid carbide precipitation. This addition of niobium makes the metals more expensive compared to a 304 and 316 [23].
- 253MA and 800H are more specialized austenitic stainless steel. In addition to the basic components such as chromium, nickel and manganese 253MA contains rare elements and nitrogen, while 800H includes titanium, aluminum and copper. These additional elements make both metals the most expensive to produce among this selection. However, 253 MA is known for its strength, especially at high temperature and, its good resistance to corrosion cracking. In contrast 800H is primarily used in applications that require excellent resistance to nitriding and carburization [24, 25].

	C	Cr	Fe	Mn	Ni	P	Si	S	Mo	Nb+Ta	Ce	N	Ti	Al	Cu
304 [26]	≤0.08	18-20	bal.	≤2	8-10	≤0.045	≤1	≤0.03	–	–	–	–	–	–	–
310S [27]	≤0.08	24-26	bal.	≤2	19-22	≤0.045	≤1.5	≤0.03	–	–	–	–	–	–	–
316L [28]	≤0.03	16-18	bal.	≤2	10-14	≤0.045	≤1	≤0.03	2-3	–	–	–	–	–	–
347 [29]	≤0.08	17	bal.	≤2	11	≤0.045	≤1	≤0.03	–	0.8	–	–	–	–	–
253MA [30]	0.08	21	bal.	≤0.8	10-12	≤0.04	≤1.6	≤0.03	–	–	0.05	0.17	0.15-0.60	–	–
800H [31]	0.06-0.10	19-23	bal.	≤1.5	30-35	≤0.045	≤1	≤0.015	–	–	–	–	0.15-0.60	0.15-0.60	0.75

Table 2.1: Composition of the Austenitic Stainless Steel used in the experimental phase (weight %).

2.2 High Temperature Oxidation

Corrosion is the phenomenon described as "*material or metal deterioration or surface damage in an aggressive environment*" [32]. Corrosion is not identified by a single phenomenon, in fact, it is considered a general term. Different types of corrosion can be identified, such as atmospheric corrosion, high temperature corrosion, liquid metal corrosion or molten salt corrosion. In this report we will focus only on the high temperature corrosion that occurs over metal plates [32].

When discussing high temperature corrosion, we refer to the tendency of a metallic material to form an oxide layer, scale or any other reaction products on their surface because of exposure to elevated temperature [33]. The formation of the oxide scale is explained by the Wagner oxidation theory, which states that the oxide layer does not grow exclusively in a singular direction. Instead, it develops both outwards from the metal surface and inward from the oxide scale, resulting in simultaneous growth at both interfaces. The reactions describing the formation of a generic metal oxide scale MO are:

$$\mathrm{M} \longrightarrow \mathrm{M}^2 + 2\,\mathrm{e}^- \text{ at the metal/oxide interface}$$
$$\tfrac{1}{2}\mathrm{O}_2 + 2\,\mathrm{e}^- \longrightarrow \mathrm{O}^{2-} \text{ at the oxide/metal interface}$$
$$\mathrm{M} + \tfrac{1}{2}\mathrm{O}_2 \longrightarrow \mathrm{MO} \text{ (overall reaction) [34]}$$

As oxygen molecules outside the oxide layer are reduced to ions, O^{2-}, these ions will diffuse inward towards the metal surface, where they react with metal ions to form the oxide scale, as shown in Figure 2.2 [34].

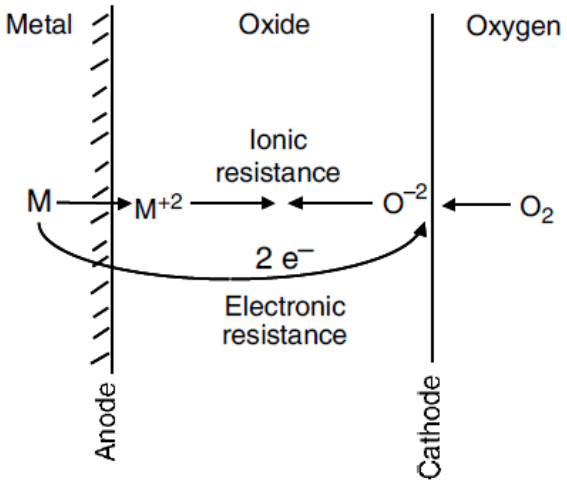


Figure 2.2: schematic representation of the oxide layer as a ionic and electronic conductor [34].

The oxide layer is therefore both a ionic and electronic conductor. However, ions and cations do not diffuse with equal freedom between the two surfaces. The extent of diffusion depends on the nature of the oxide. In the case of chromium or iron oxides, cations tend to diffuse outward more easily and significantly than the anions [34]. To enable the movement of cations or anions, a large negative gradient of free energy is necessary. This gradient of free energy, also known as the standard free energy change ΔG°, is determined under equilibrium conditions:

$$\Delta G^\circ = RTln(pO_2)(g)$$

Where $pO_2(g)$ represents the partial pressure of oxygen at a given temperature T, and R is the gas constant. The dissociation pressure of oxygen can be calculated directly from this formula. By plotting the resulting ΔG° against temperature, one obtains the dissociation pressure for specific metal. This type of graph is called Ellingham graph and it is shown in Figure 2.3. However, the Ellingham graph only indicates the necessary temperature and pressure conditions to initiate the oxidation process, it does not provide information about the rate of the process itself [33].

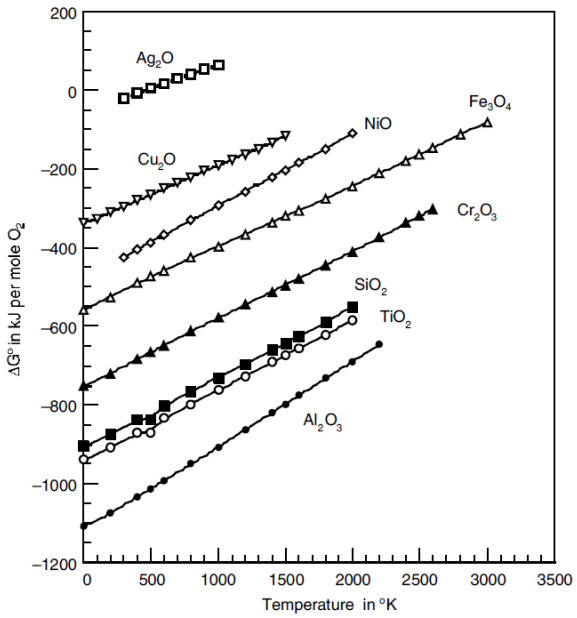


Figure 2.3: Ellingham graph, showing the energy of formation of different oxides [34].

To better understand the oxidation process at high temperature and to predict it as accurately as possible, is important when designing material for engineers' purpose, especially those intended for high temperature application. For this reason, it is necessary to introduce time as a variable, thus oxidation kinetics must be considered. The oxidation kinetic describes the rate of the oxidation process over time. Three behaviors can be observed: linear, parabolic and logarithmic [33].

These three laws describe how materials can oxidize at high temperature, each following a different pattern. The most common rule observed for metal and alloys at high temperatures is the parabolic law: the rate of oxide layer formation decreases over time, meaning the growth rate is inversely proportional to time. In contrast, with the logarithmic law, there is a high oxidation rate at the beginning, followed by a very slow rate of oxidation as time progresses. The linear law is the worst-case scenario for oxidation: the formation of the oxide layer is directly proportional to time,

meaning that the oxide layer does not protect the material but it is just a porous layer letting the O_2 through. As the heavy oxide layer forms and eventually falls off, the material is exposed again, and oxidation restarts, leading to rapid material degradation [33]. The three laws are shown in Figure 2.4.

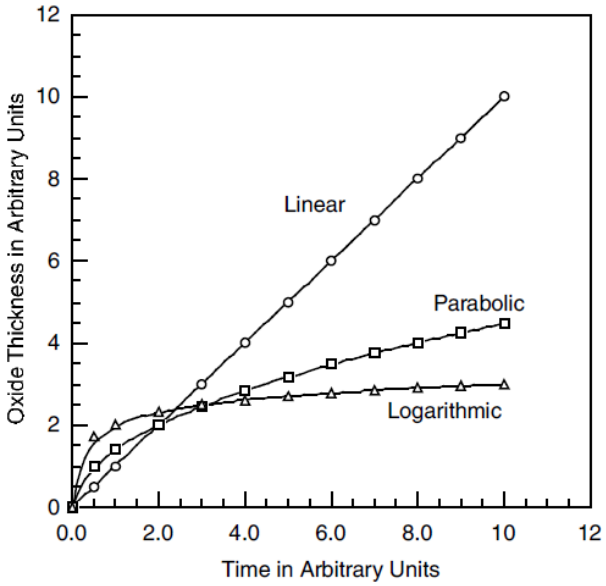


Figure 2.4: Graphic representation of three oxidation kinetic laws [34].

2.2.1 Oxide film in austenitic stainless steels

During high temperature oxidation, materials are designed to withstand corrosion by forming a protective oxide layer or, in some cases, by applying a protective coating. Austenitic stainless steels form a protective chromium oxide Cr_2O_3 through passivation, which acts as a barrier against further oxidation and corrosion.

A schematic explanation of the different oxide scales formed based on chromium concentration is presented in Figure 2.5. As can be observed, when there is only a small amount of chromium presence, iron oxide, also known as rust, is the main oxide formed. In contrast, for achieving the complete and optimal corrosion-resistance layer of chromium oxide, at least 18% is required [20].

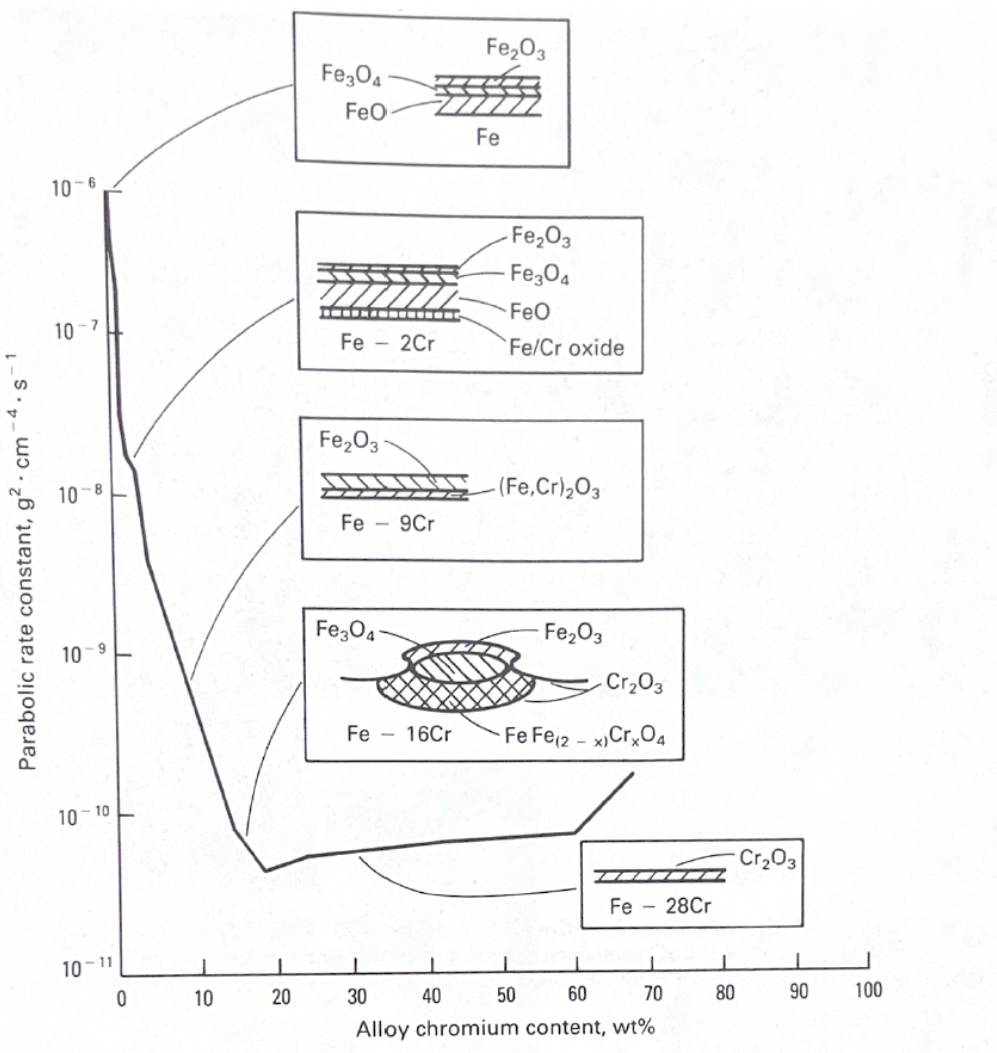


Figure 2.5: Variation of the oxide layer formed at 1000 C based on the amount of chromium [34].

2.2.2 Chromium depletion layer (CDL)

The chromium depletion layer (CDL) occurs between the oxide scale and the base material. This region is characterized by a lower chromium content than the original matrix material, as chromium is consumed in the formation of the oxide scale. The role and the development of the chromium depletion zone in relation to the different stages of oxidation has not yet been thoroughly studied. However, since the chromium depletion starts at grain boundaries, it is possible that grain boundaries engineering can significantly influence this phenomenon [35, 36] .

It has already been established that the chromium depletion layer forms from the initial stage of oxidation, as chromium oxidizes with oxygen to create the oxide scale. Because the formation of the oxide scale is governed by the diffusion rate, as previously discussed, it is highly probable that the chromium depletion layer is controlled by the same physical principle. There may also be a correlation between the chromium depletion layer, and the thickness of the material is presented, but this topic requires further investigation [35].

2.3 Descaling Method

The descaling process refers to the removal of the oxide layer that forms over the base material of stainless steel after prolonged exposure at high temperatures. Unfortunately, as previously mentioned, the literature on descaling is limited and often focuses on specific applications. It is possible to identify different types of descaling process: chemical, mechanical, ultrasonic, thermal and electrochemical, as shown in Figure 2.6. In this dissertation, the focus will be primarily on chemical and mechanical descaling methods, as a combination of these two processes was employed during the experimental phase [37].



Figure 2.6: Overview of different descaling methods [37].

2.3.1 Chemical descaling and pickling

Chemical descaling refers to the process of using an aqueous solution in order to remove the oxide layer. Pickling is a specific type of chemical descaling in which the acid solution removes the oxide layer but helps to passivate the descaled surface. Passivation is a chemical process that forms a chromium oxide layer on stainless steel, which gives the material its oxide resistance [38].

During the pickling process of stainless steel, the four main acids used are nitric acid (HNO_3), hydrofluoric acid (HF), sulfuric acid (H_2SO_4), and hydrochloric acid (HCl). Nitric acid is the most commonly used component in descaling solutions, as it helps preserve the chromium layer that gives the austenitic stainless steel its corrosion resistance, rather than destroying it. The other three acids mentioned, hydrofluoric, sulfuric, and hydrochloric acid, are used in the solution to remove the oxide layer and allow for effective descaling of the surface. The most common descaling solution for austenitic stainless steel is prepared by mixing in an aqueous solution 10-15% nitric acid with 1-3% of hydrofluoric acid in distilled water. The concentration of hydrofluoric acid is typically adjusted based on the thickness of the oxide scale, which, for austenitic stainless steel, is primarily chromium oxide, Cr_2O_3. This solution is usually applied at elevated temperatures, between 50-60°C. If used at room temperature, the process may take longer to be effective, and

higher concentration of acid may be required. It is important to note that different types of stainless steel require different descaling solutions [11, 39] .

Pickling and chemical descaling are broad topics, as both the nature of the oxide layer and the base material can vary greatly, leading to different reactions. Many studies have been conducted, and different solutions have been developed. Often, more than one step is required, and different guidelines have been established [40, 41].

Chemical descaling usually proceeds in three stages: dissolution, reduction and peeling. Dissolution represents the first stage of the process, when the oxidized material is exposed to the acid solution and the oxide scale that has formed on the surface begins to dissolve. However, at this stage, it is still not possible to completely remove the oxide scale. During the reduction stage, some of the hydrogen atoms that have penetrated the base material and the CDL help dissolve the oxide still preset after the dissolution phase. Peeling is the final stage of chemical descaling, occurring when the whole oxide scale is sufficiently loosened to be simply peeled off from the base material or the CDL [35].

2.3.2 Mechanical Descaling

Mechanical descaling represents for the majority of cases documenting the mechanical action of removing the layer through a brush. Almost no literature is presented which gives more specification over the kind of brush or movement. Of course, based on the application of mechanical descaling the technique may vary, as if the object continued to be used after the process it may be important to avoid scratches, in some cases study the direction of the brushes became an important factor to account while descale [42].

Chapter 3

Methodology

In the first phase, from this point forward referred to as Phase 1, the main objective was to identify the most effective descaling method. To achieve comprehensive evaluation of the process tested, six different austenitic stainless steel with a different chemical composition were selected, (the six materials selected have been introduced and analyzed in *Literature review* chapter 2.1.3). This approach made it possible to investigate a diverse and manageable range of materials providing valuable insights into potential directions for future research.

To maintain the validity of the experimental results, three samples of each material were exposed to four different high temperatures: 600°C, 680°C, 800°C, and 950°C. Each sample was subjected to the same exposure duration at each temperature. This method enables the comparison of the two-descaling methods across different temperatures and materials. In the second phase, as referred to Phase 2, the focus was shifted to a more comprehensive analysis. After the descaling method was evaluated and found to be sufficiently reliable for the selected set of materials (304, 310S, 316L and 347), an adequate number of samples was prepared to study the oxidation kinetics at two fixed temperatures: 800°C and 600°C.

The parameters and materials used during Phase 1 and Phase 2 are shown in table 3.1.

Phase 1	
Materials	304, 310S, 316L, 347, 253MA, 800H
Temperatures	600°C, 680°C, 800°C, 900°C
Exposure Time	117 h
Phase 2	
Materials	304, 310S, 316L, 347
Temperatures	600°C, 800°C
Total Exposure Time	2011 h
Extraction time (h)	$\approx$ 250 h (800°C), $\approx$ 500 h (600°C)
Extraction time (days)	$\approx$ 10 days, $\approx$ 20 days

Table 3.1: Parameters and Materials used in Phase 1 and Phase 2.

3.1 Sample preparation

Samples for both experimental phases were manually cut. The thickest plate was the 304 stainless steel, with a thickness of 2 mm. Cutting was performed using a Struers metallographic cut-off machine, model DISCOTOM 10, available in the metal laboratory. For all the other austenitic stainless steel samples, which had thicknesses ranging from 0.38 mm to 0.83 mm, a manual shear was employed allowing for a quicker and less time-consuming cutting process.

In Phase 1, which focused on evaluating the effectiveness of the descaling methods, larger samples, approximately 6 $mm \times 4$ mm, were prepared whenever possible, to maximize the area exposed to the acid. However, for 353MA and 800H, which were received as narrow strips, the samples were cut to 2 $mm \times 7$ mm. In contrast, during Phase 2, samples used for determination of the oxidation kinetic curve, were made smaller to optimize the use of the available material with the measurement approximately between 2 $mm \times 7$ mm.

After cutting, all samples were measured through an electronic caliper in every direction. Since most cuts were made manually, perfect precision could not be guaranteed resulting in minor deviations. However, this did not effect the reliability of the results, as the measurements were normalized in the following calculations. All the samples were then weight with an analytical scale Mettler Toledo XS204 before being placed in the furnace. The precision of the scale was on the order of 0.0001 g, as shown on Figure 3.1, since the weight changes observed after an oxidation cycle were in milligram range, differences too small to be detected by a standard laboratory scale. The sample weights varied depending on the material's thickness was different, ranging from the ≈1g to ≈20g.



Figure 3.1: 304 sample on the precision scale after extraction from the oxidation furnace.

3.2 The furnaces

The oxidizing furnaces used throughout the entire experiment are shown in Figure 3.2. The largest furnace (Figure3.2a) has a capacity of 40 liters. It is part of the Muffle furnaces series by Nabertherm and can reach temperatures up to 1100 °C. The smallest furnace (Figure 3.2b)is an Entech EEF 3/17, with a capacity of only 4,1 liter and can reach temperatures to 1700°C. During both experimental phases, the two furnaces were operated simultaneously. During Phase 1, the furnaces were operated for a fixed duration of 117 hours, which corresponds to the oxidation cycle time for each temperature. During Phase 2, the Muffle furnace, due to its greater capacity, was used for the oxidation of a larger number of samples at the fixed temperature of 800°C (Figure 3.3a). The EFF furnace was also operated simultaneously (Figure 3.4) at the fixed temperature of 600°C. The oxidizing cycle in both furnaces lasted approximately 2000 hours.



(a) Muffle Furnace.

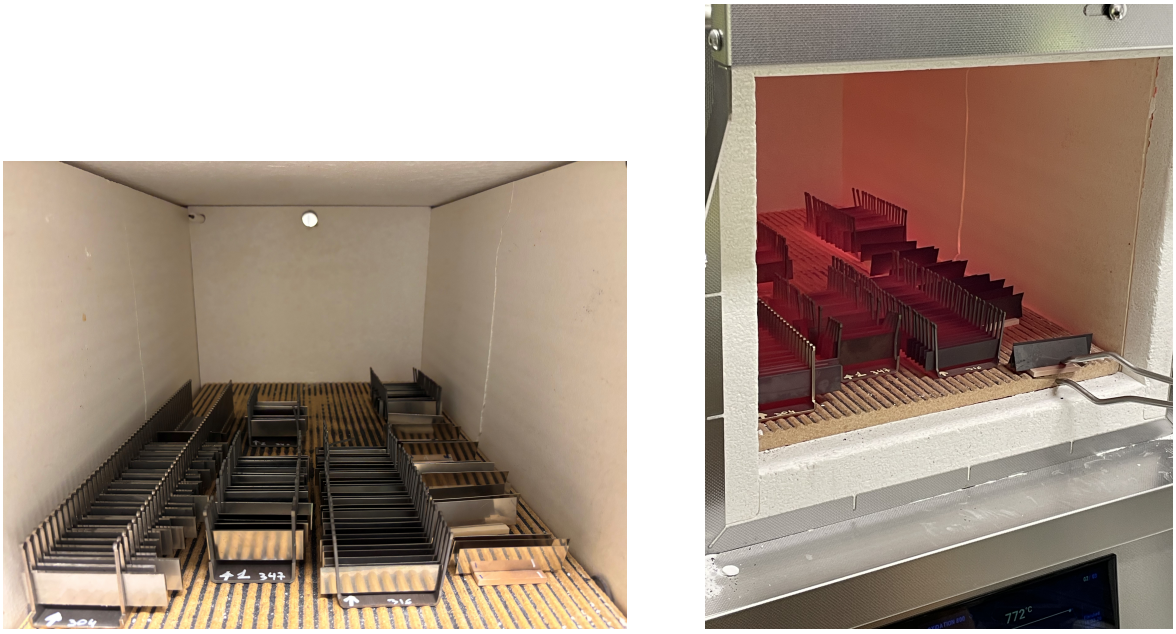
(b) EFF Furnace.

Figure 3.2: Furnaces used in the experimental phases.

To study the oxidation kinetic at 800°C more extensively and obtaining a more detailed model, 30 samples for each material were loaded into the Muffle furnace. Given the significant number of samples, they were divided into different labeled holders based on material type and positioned inside the furnace to facilitate the extraction (Figure 3.3a). Three samples per material were extracted approximately every 10 days, about 250 hours, without stopping the operation of the furnace (Figure 3.3b).

The oxidation kinetic was also studied, less extensively, at 600°C. Due to the spatial constraints in the EFF furnace only 12 sample per material were loaded inside the furnace and 347 was excluded as a material of interest at this temperature (Figure 3.4). Extractions occurred approximately

every 20 days, about 500 hours. As in the previews case, the furnace remain operating throughout all extractions.



(a) Loaded furnace - 800℃.

(b) Samples extraction.

Figure 3.3: Muffle Furnace used during Phase 2.

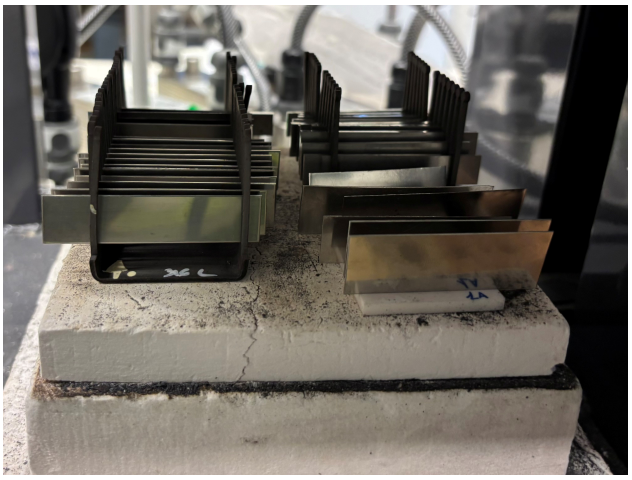


Figure 3.4: EFF furnace loaded during Phase 2.

3.3 Descaling Process

Two solutions were used in Phase 1. The preparation of these solutions was based on previous work and a literature review (2.3.1). The preexisting research conducted in the Alfa Laval's department was continued and further developed in this study.

Solution A was an aqueous solution prepared by mixing 15-20% nitric acid (HNO_3), with 1-3% rock salt (NaCl). Solution B was obtained by combining 15-20% nitric acid (HNO_3) and adding 1-3% hydrofluoric acid (HF). Both solutions were prepared in advance and under supervision, as both nitric acid and hydrofluoric acid are hazardous substances, and they must be handled according to safety procedures. For this reason the solutions were stored in a ventilated cabinet and handled inside the fume hood during the experiments.

Phase 1 was designed to asses which solution between Solution A and Solution B, was most effective at descaling the oxidized samples. To achieve this, the sample were weighted again after the extraction. Two out of the three oxidized sample were then immersed, one in a glass beaker containing Solution A (Figure 3.5a) and the other in a plastic container containing Solution B (Figure 3.5b). Solution B is more corrosive than solution A and it could have damaged the glass beaker, compromising handling safety.



(a) Descaling sample Solution A - Starting. (b) Descaling sample Solution B - Starting.

Figure 3.5: Starting of the descaling process Phase 1.

Once the samples were immersed in the solution, they were visually inspected, since a good indicator of the progress of descaling process was the change in color of the solution (Figure 3.6). In fact, the darker the solution became, the more quickly the descaling process was happening. When, based on visual evaluation, the oxide appeared sufficiently loosened, the sample was removed from the container depending on the solution and any visible oxide residues were removed using a kitchen cleaning brush. After descaling, the samples were rinsed with distilled water and weighed again to determine the mass change due to the loss of the oxide layer. In addition, the time required by each solution to descaled the different samples was recorded, as the company required the descaling process to be completed under 6 hours.

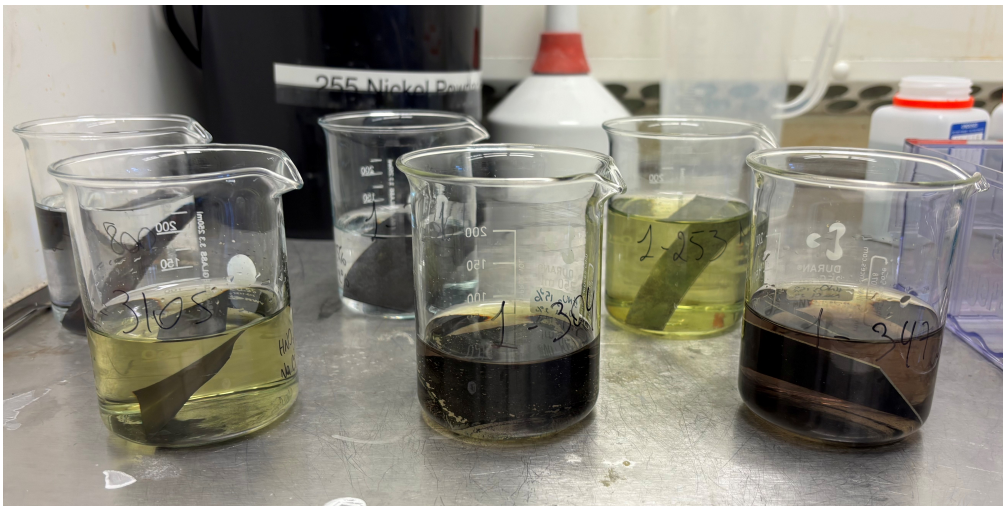


Figure 3.6: Color difference in Solution A due to the different stages the sample are in the descaling process.

In Phase 2 the descaling method established during Phase 1 was applied to a larger group of samples (Figure 3.7). The samples were weighted after extraction, immersed in the solution, visually inspected, cleaned with a kitchen brush, rinsed with distilled water, and then weighed again. The time required for descaling was also recorded. The descaling solutions were reused during some of the processes, to avoid unnecessary wasted of chemical agents. The main difference from the previous Phase was the use of only Solution B for descaling the samples. This decision was based on practical considerations: Solution B showed faster descaling times for all the materials compared to solution A, and time was a significant constraint throughout the experiments.

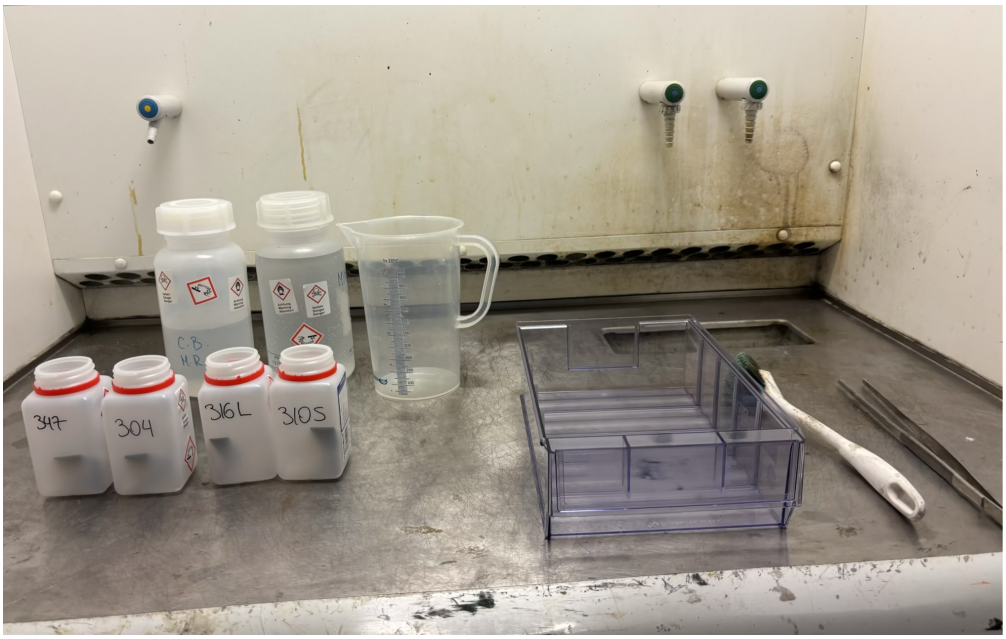


Figure 3.7: Starting station for the descaling process in Phase 2.

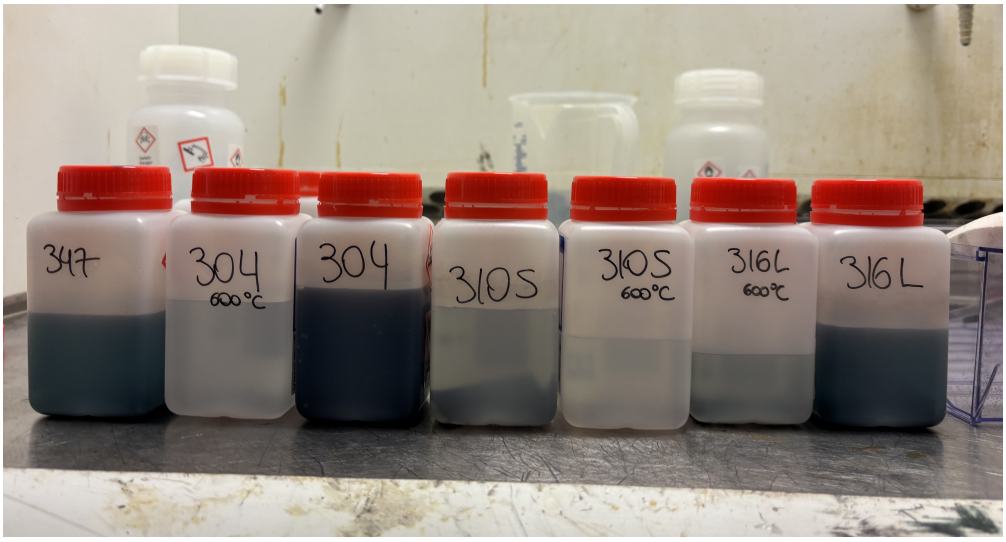


Figure 3.8: Samples in different descaling stages during Phase 2.

The organization of the solution containers was improved during the project: the solution used for descaling a specific material was used exclusively for that material and, in Phase 2, the plastic containers were prepared in advance, each clearly labeled with the name of the material descaled and all the relevant safety information.

3.4 Sample preparation: cross section and mounting

After Phase 1 and Phase 2, a significant amount of samples were available for analysis. Due to the large quantity, it was decided to focus only on those from Phase 1, as they underwent four different oxidizing temperatures and they were descaled by both solutions. This approach made possible to study both the oxide layer and its variation across different temperatures, as well as the impact of the descaling solutions and the conditions of the base material after descaling. In order to compare and analyze the different materials, it was decided to prepare a cross section of each sample.

A cross section, which is a perpendicular cut to the surface, allows for the examination of both the surface layer and the base material. To obtain the cross section, the samples were cut following the same method described in the "*Sample Preparation*" 3.1. Once again, the thickest samples were cut through the Struers metallographic cut-off machine, model DISCOTOM 10, while the other samples were cut using a manual shear. Each sample was cut to approximately 10 mm in length. Samples of the same material, oxidized at the same temperature, were mounted together in a holder, with three samples per holder (Figure 3.9). Mounting was performed manually using an epoxy resin. After hardening, the mounted samples were grounded and polished according to the standard procedure using the Struers Polisher (LaboForce 100) polishing machine.

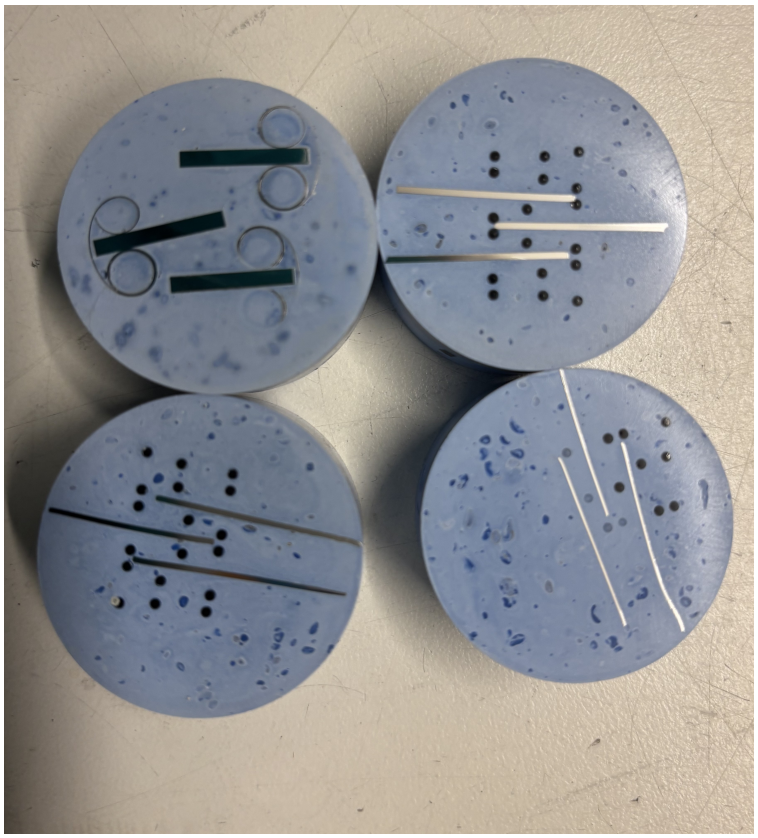


Figure 3.9: Mounted samples in the epoxy resin.

Chapter 4

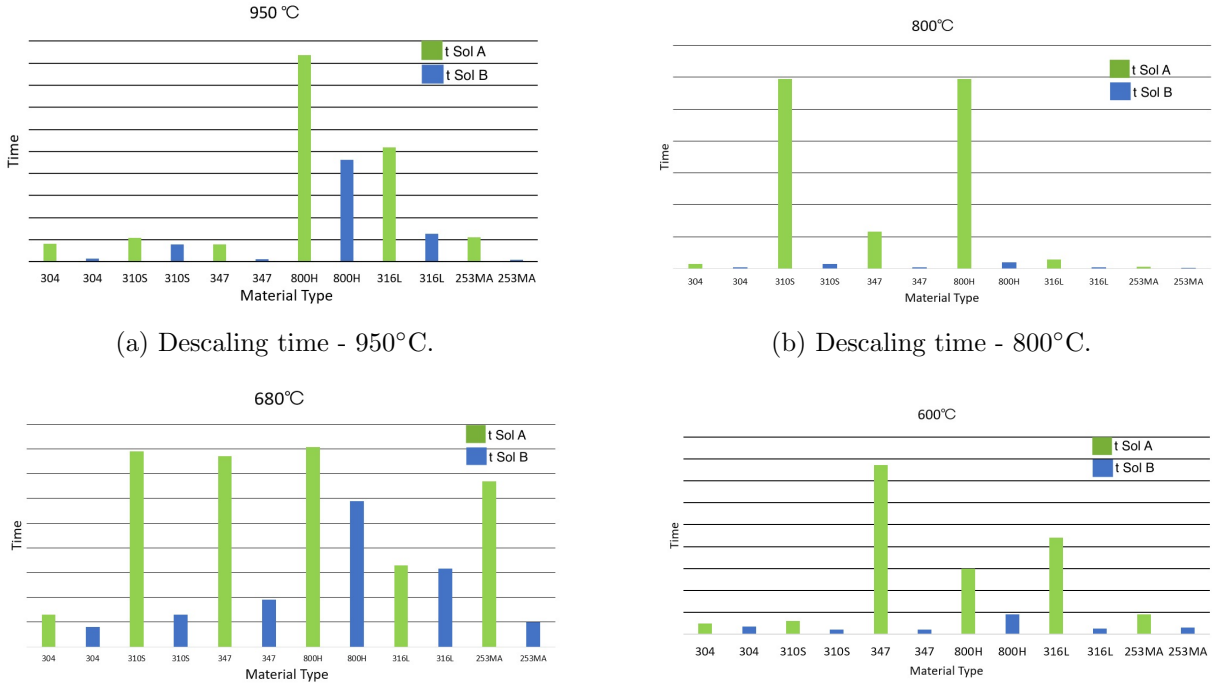
Results and Discussion

In this chapter, the results collected throughout the entire thesis project will be presented. The discussion begins with a brief overview between the descaling behavior and the time required for the samples to be cleaned. The discussion then moves to a comparison between the work carried out during these months and the results from a previous study conducted in the same Alfa Laval's department, which investigated the mass gained at different oxidation temperatures. Even though only one temperature, 600°C, used in the two studies is the same, this comparison provides a starting point for the following discussion and a validation of the results. Before presenting the actual oxidation kinetics behavior for thickness loss over time at the two different temperature, the samples from Phase 1 will be examined using both stereoscopic microscope and optical microscope.

4.1 Descaling behavior: time observation

As previously mentioned, the time required for each descaling process was recorded to collect data about the procedure itself and to compare the difference between the materials, the solutions and the oxidation temperatures. In Phase 1, the main focus was on finding which solution was both the most effective in descaling the surface and the least time consuming, while in Phase 2, additional data were collected, placing more importance on the oxidation time, as the temperature remained fixed.

Figure 4.1 shows the different descaling time recorded during Phase 1. The green bars represent the time required to descale the samples using Solution A, while the blue bars indicate the time required with Solution B.



(a) Descaling time - 950°C.

(b) Descaling time - 800°C.

(c) Descaling time - 680°C.

(d) Descaling Time - 600°C.

Figure 4.1: Representation of the different descaling times, depending on base material, oxidation temperature and descaling solutions. Green and blue bars represent the different solutions A and B, respectively.

The main trend outlined from Figure 4.1 is that Solution B tends to be more effective in term of descaling time than Solution A. Across all temperatures and materials, the solution containing hydrofluoric acids, Solution B, generally removes the oxide scale faster than the rock salt solution, Solution A. However, this leaves room for future research into more sustainable, less aggressive and less hazardous descaling methods. For example, 304 stainless steel showed good results in both solutions, as does 253 MA. On the other hand 800H is extremely complex to descale, particularly with solution A. Among the group of materials selected, 800H is one of the most highly alloyed austenitic stainless steels. It is plausible that titanium nitride forms in the base material as another study suggests [43]. Other important materials, which will be central in Phase 2, such as 310S and 347, exhibited longer descaling time with solution A especially at 800°C. For these reasons, only Solution B was used in Phase 2.

For Phase 2, no Figure about the recorded time are presented, as the materials generally showed a tendency to stabilize the time required to remove the oxide scale. The only exception was 316L at 800°C, which showed an increase in descaling time with longer oxidation exposure.

4.2 Mass measurement

When investigating oxidation, an important parameter to consider is the mass of the sample. During an oxidation cycle, a change in the mass from the initial value is usually observed. By measuring this difference, it is possible to calculate the mass gain per area.

Studies on mass gain per unit area have already been conducted by Alfa Laval department in a

previous thesis project [44], and these represented the starting point for these analysis, in order to understand what what went wrong and what could be implemented. The previous project focused on a parameter recognized by scientific literature but difficult to apply in real life scenario. Mass gained per area, typically expressed in mg/cm^2, allows for comparison of oxide layer formation between different materials. However, it does not provide any actual information about when or how the oxide scale will spall off and how, neither does it indicate how much the thickness of the original plate will decrease as a result. Having said that, to establish a starting point and enable comparison, since the data had already been collected, the mass gain per area was also calculated for the material selected for Phase 2.

When discussing oxidation behavior at high temperature, an important aspect to analyze is the oxidation kinetic behavior, as this provides the most accurate way to interpret the data and obtain valid results. Due to limitations in the previous work, this factor was not considered, however by rearranging their data based on the oxidation kinetic can support the reliability of the results. Based on these preliminary findings, the data collected were used as a starting point to calculate the most realistic behavior based on the three oxidation kinetic explained in the "*High Temperature Oxidation*" 2.2 . The trend which showed the lowest mean squared error was chosen as the most reliable. These graphs were also used to investigate whether any correlation could be found between mass gain per area and thickness loss over time.

The Figure 4.2 shows the mass gain per area over time at 800°C. Among the materials tested, 304 experiences the fastest corrosion rate. This is likely due to its chemical composition, 304 is characterized by a simpler formulation compared to the other austenitic stainless steel studied. When comparing the weight percentage of 347 and 316L with 304, they both contain less carbon but include additional elements that enhance protection at 800°C. Specifically, 316L contains molybdenum, which improves corrosion resistance [20], while 347 is enriched with elements such as niobium and tantalum, which act as stabilizers of the structure, enhancing high temperature performance [14, 13]. 310S has the highest chromium, nickel and silicon content by weight percentage among all the materials tested, which enhances its corrosion resistance, especially when exposed to a high temperature corrosion environment [22]. For the reasons explained above, 310S and 347 exhibit the lowest corrosion rate, followed by 316L.

As it is possible to observe in Figure 4.2, all the materials at this temperature exhibit a parabolic behavior of mass gained per area over time. These results are based on the analysis of the data collected throughout Phase 2. In fact, the model that exhibit the lowest squared error is the one the best approximate reality. However, this will be explained further when analyzing the thickness loss over time of the material.

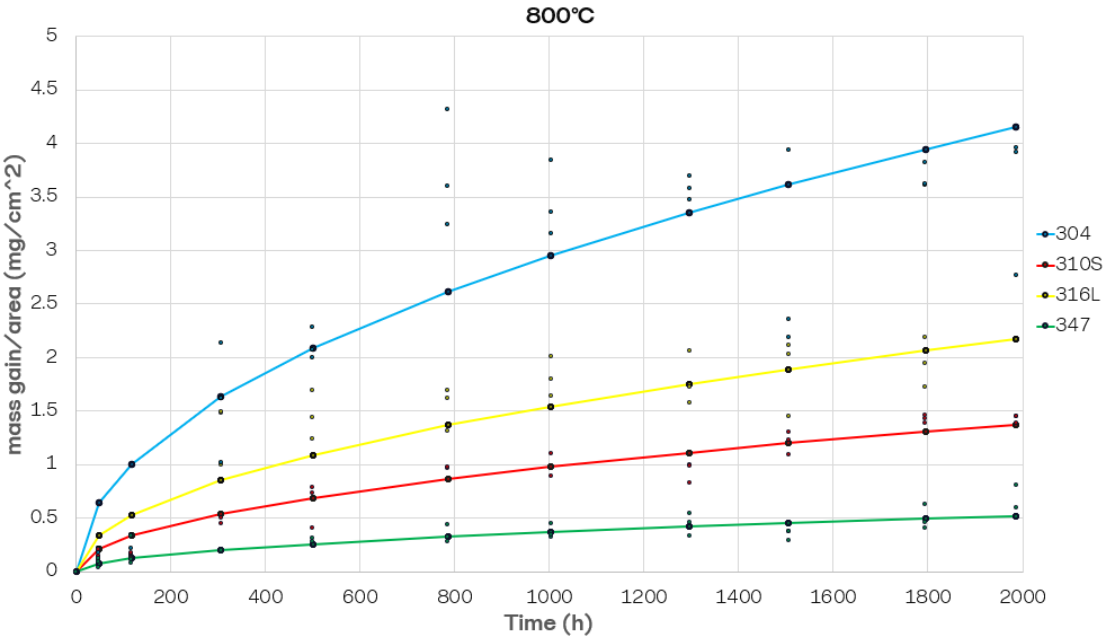


Figure 4.2: Mass gained per area over time at an oxidation temperature of 800 °C.

At 600 °C, as shown in the Figure 4.3, it can be observed the situation appears different, as the three materials display different corrosion rate. Among them, 304 is the only material that exhibits a logarithmic model, while 310S and 316L display a parabolic trend in gaining weight. At this temperature, 310S shows the lowest corrosion rate, followed by 304, with both gaining less than 0.2 mg/cm^2. 316L exhibits the highest corrosion rate gaining more than 1 mg/cm^2 in almost 2000 hours. The overall mass gained over time is reduced compared to that recorded at 800°C due to the temperature being 200°C lower.

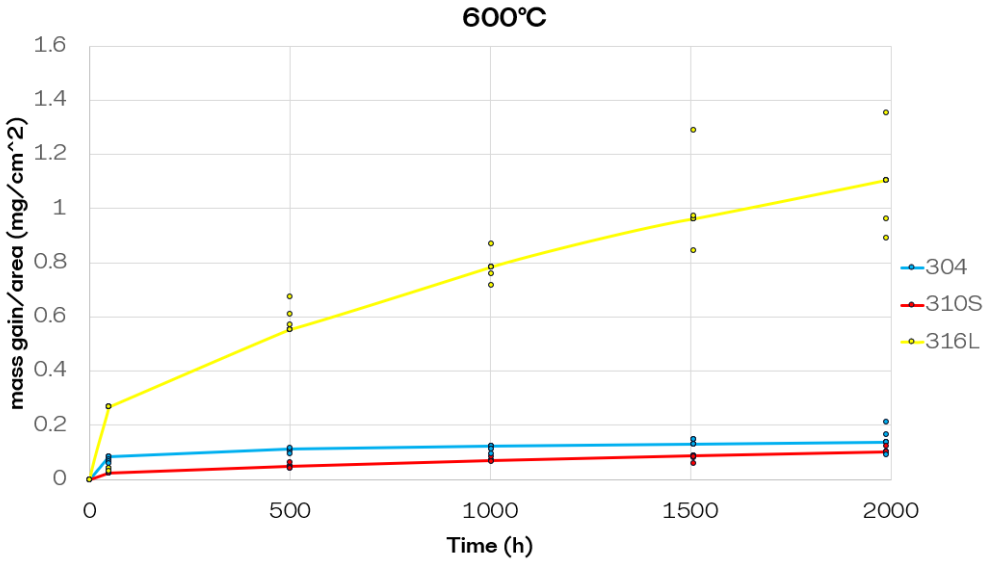


Figure 4.3: Mass gained per area over time at an oxidation temperature of 600 °C.

When comparing the mass gained over time of the materials at the two tested temperatures, a general trend was noticed in their behavior during the oxidation cycle. 316L exhibits the poorest overall performance in terms of corrosion rate. In fact, the difference in mass gain per area over time between 800°C 600°C is only 36%. This might be due to some spallation of the oxide layer or localized corrosion. Visual inspection of the 316L samples after longer furnace cycle showed that the oxide film formed was inhomogeneous, with some areas appearing darker and others lighter, as shown in Figure 4.4.

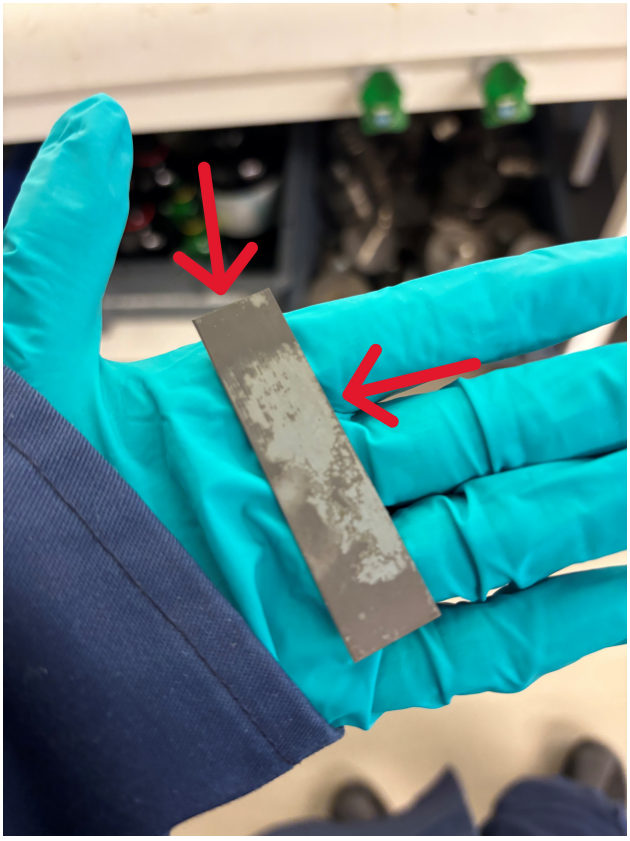


Figure 4.4: 316L sample before descaling process showing an inhomogeneous oxide layer.

As previously mentioned, some data had already been collected in a prior project [44]. Due to limitations, 800°C was not considered as a service temperature and for 600°C, the data was collected for only 450 hours, without including 304 as a material of interest. The data were not presented as they are now, at the time, it was decided to use the average values collected to plot the curve. Despite these limitations, it was still possible to observe whether the trends of 316L and 310S were similar or completely different from those observed in the data collected in Phase 2, and the trends matched for both materials.

316 L, as shown in the Figure 4.5, exhibits a linear fitting curve in both cases. The difference in mass gained over area area between the two data sets is approximately 0.1 mg/cm^2, a difference that could be consider negligible due to its small magnitude. The data from the previous work provide a more accurate curve as more data points were collected within that time frame.

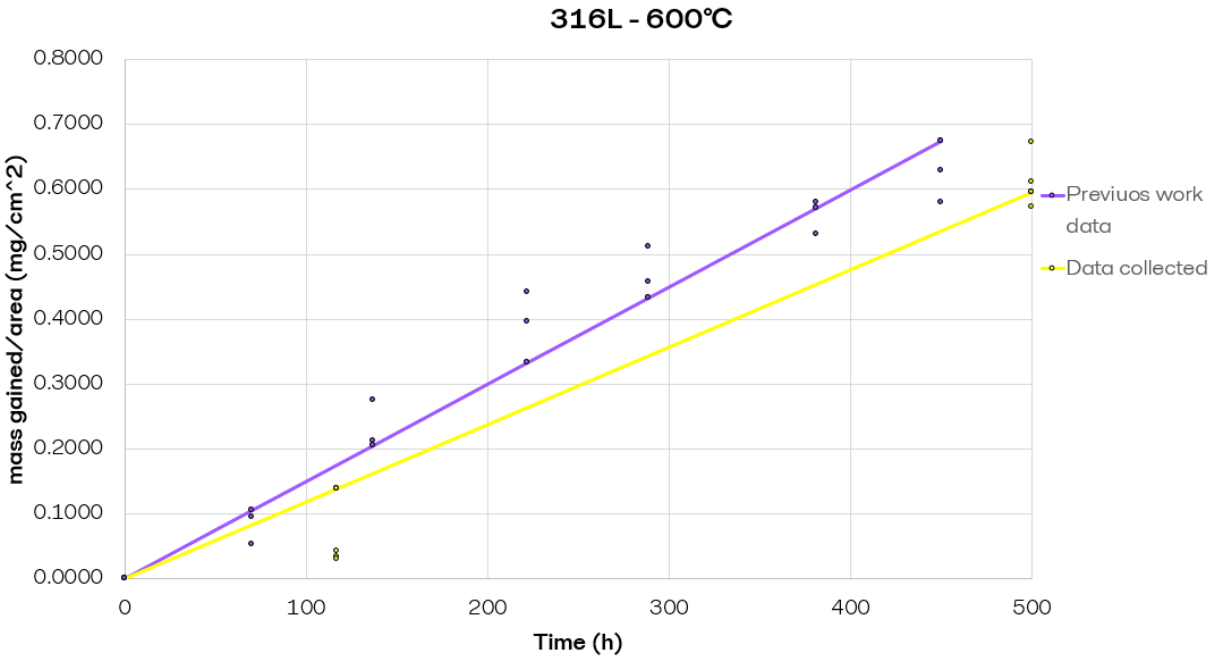


Figure 4.5: 316L comparison weight gained over area at an oxidation temperature of 600°C.

Similar observations can be made also when comparing the data sets for 310S, as displayed in the Figure 4.6. When plotting the data from the previous work alongside the data collected in this study, the material exhibits a logarithmic trend in both cases. Moreover, as with 316L, the difference between the two curve can be consider negligible as in the magnitude of less than $1 mg/cm^2$. The results obtained for both materials indicates their reliability, as the two experiment where carried out with almost two years apart.

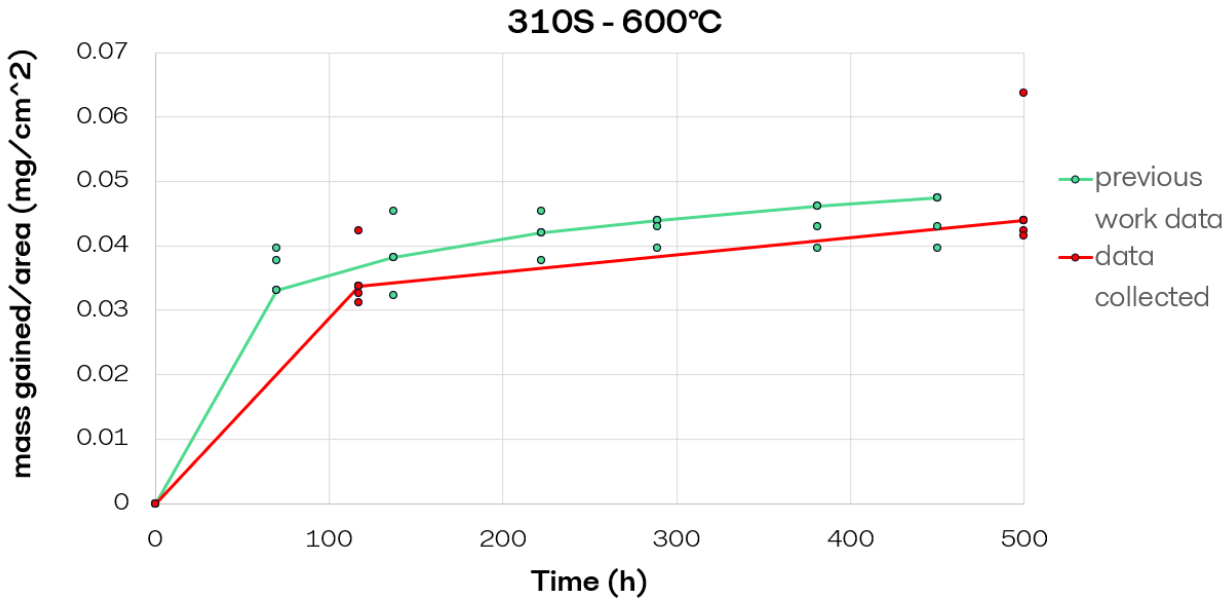


Figure 4.6: 310S comparison weight gained over area at an oxidation temperature of 600°C.

4.3 Stereoscopic microscope analysis

The stereoscopic microscope is a type of low magnification microscope that allows to capture detailed images with a high depth of field [45]. For this report, the Leica M205C encoded stereo microscope present in the metal laboratory was used to obtain a preliminary visual evaluation of the samples' surface after descaling and oxidation. Samples that had undergone descaling with the two different solutions were compared with each other, as well with those that had only undergone oxidation. This approach was adopted to establish a methodology for future work. This procedure was repeated for each temperature investigated in Phase 1, and the pictures were taken before cutting and mounting the samples in the holder. In this report only the image regarding the four materials studied in Phase 2 will be presented.

Figure 4.7, to 4.10, provide an overview of the samples descaled with Solution A compared to those descaled with Solution B after exposure to different oxidizing temperatures. All the sub-figures, the samples descaled with Solution A are shown on the left, while the samples descaled with Solution B are shown on the right. As observed in the Figures 4.7a to 4.10a, 950°C resulted in the most difficult oxide scale to dissolve, especially with solution A. While, after undergoing the oxidizing temperatures of 680°C and 600°C, Figures 4.7c to 4.10c and figures 4.7d to 4.10d, both solutions demonstrated good descaling performance, as almost no oxide layer is visible.

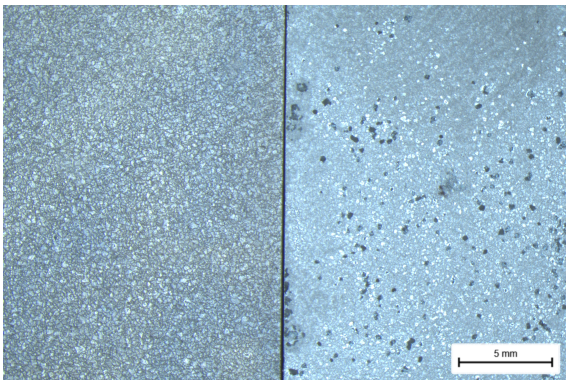
Among the materials tested, 310S exhibited the poorest performance in term of descaling with solution A, especially after oxidation the two most critical temperatures of 950°C and 800°C. In fact, as it possible to notice in Figure 4.8a and 4.8b, significant residues of the oxide layer, the black areas on the samples, remained after being descaled with Solution A, compared to those descaled with solution B. This difference in the descaling efficiency between the two solutions could be cause by the composition of 310S, which has highest chromium and silicon content among the four austenitic stainless steel tested. These elements probably contribute to the formation of an oxide scale that more resistant to acid dissolution. Although all the materials develop the same oxide scale, Cr_2O_3, their bulk composition differs, which affects how the acid solution interacts during the various stages of descaling. 304 exhibits good descaling results with both solutions after all the oxidizing temperatures. 316L showed the poorest results with both solution at 950°C, while at lower temperature, the results were good with both solutions. 347 performed well at all oxidizing temperatures with Solution B, while with Solution A, it exhibited problems at 800°C and 950°C.

Another factor that may have influenced these results is the oxidation temperature, in fact the highest the temperature the greater the corrosion rate, making the samples oxidized at 800°C and 950°C more complex to descaled compared to those oxidized at 600°C and 680°C. Moreover, as previously explained, descaling was performed at room temperature to minimize operational risk. This may have slowed some interactions between the sample and the solutions.

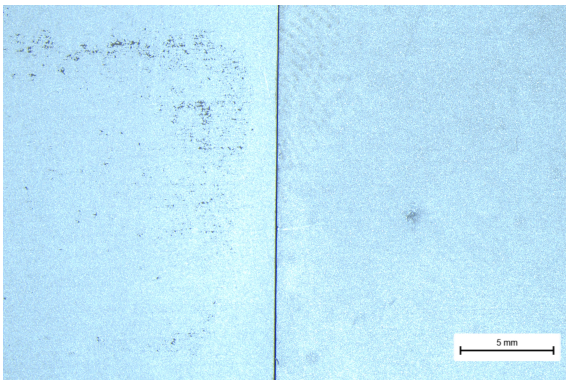
Table 4.1 provides a comprehensive summary of the results collected during Phase 1, only based on the visual inspection recorded with the stereoscopic microscope and do not take into account the time required by the solution to descale the samples.

	950°C		800°C		680°C		600°C	
	Sol. A	Sol. B	Sol. A	Sol. B	Sol. A	Sol. B	Sol. A	Sol. B
304	✓	✓	✓	✓	✓	✓	✓	✓
310S	✗	✓	✗	✓	✓	✓	✓	✓
316L	✗	✗	✓	✓	✓	✓	✓	✓
347	✗	✓	✗	✓	✓	✓	✓	✓

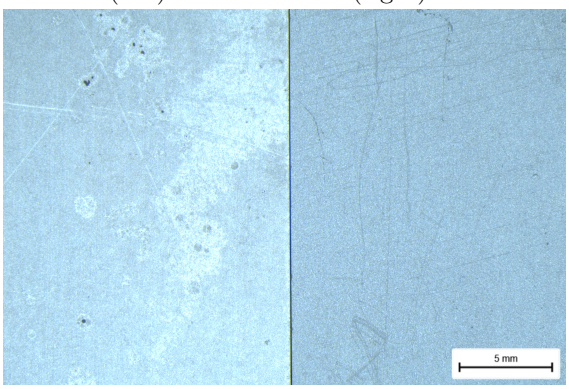
Table 4.1: Results from the data collected with the stereoscopic microscope. The ✗ symbol indicates that the descaling process was not successful. The ✓ symbol represents that the descaling process was successful.



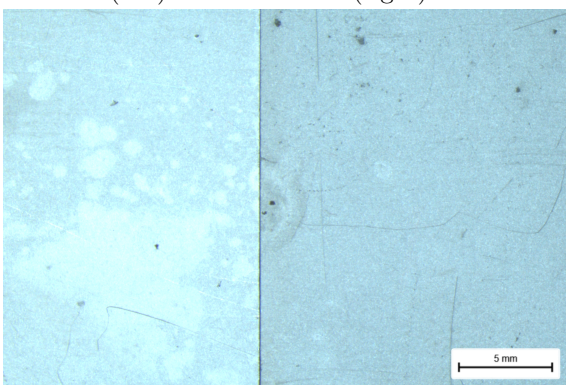
(a) Descaled 304 samples oxidized at 950°C: Solution A (left) vs. Solution B (right).



(b) Descaled 304 samples oxidized at 800°C: Solution A (left) vs. Solution B (right).

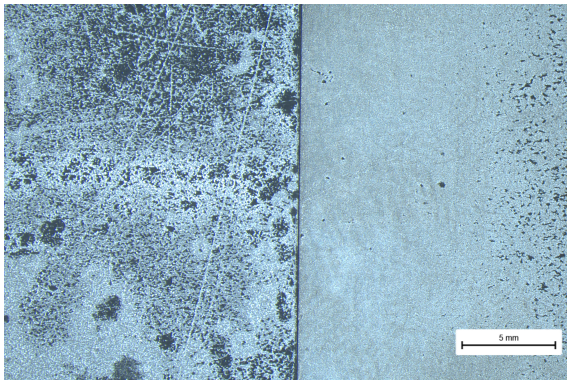


(c) Descaled 304 samples oxidized at 680°C: Solution A (left) vs. Solution B (right).

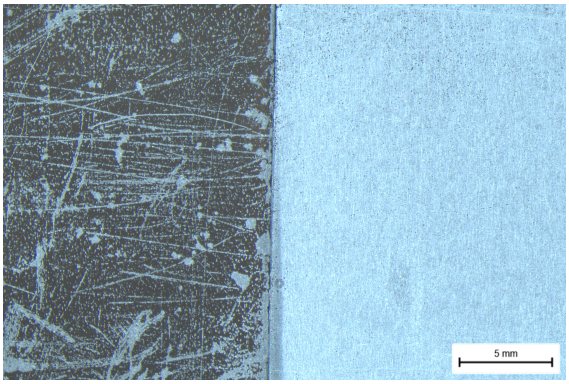


(d) Descaled 304 samples oxidized at 600°C: Solution A (left) vs. Solution B (right).

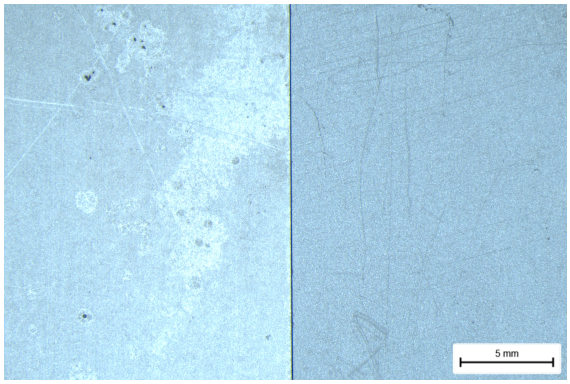
Figure 4.7: Stereoscopic images of 304 samples oxidized at different temperatures and descaled using both Solution A (left) vs. Solution B (right).



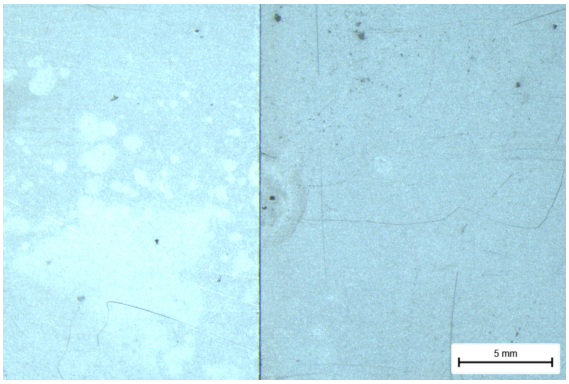
(a) Descaled 310S samples oxidized at 950°C: Solution A (left) vs. Solution B (right).



(b) Descaled 310S samples oxidized at 800°C: Solution A (left) vs. Solution B (right).

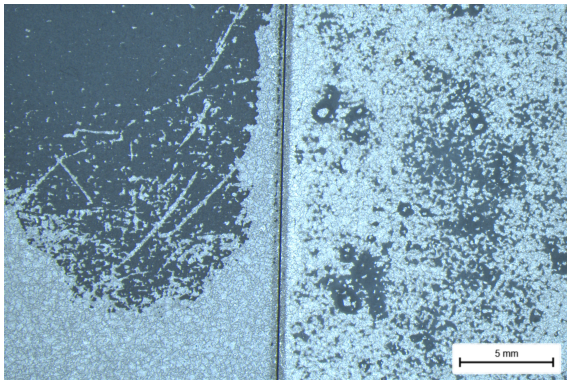


(c) Descaled 310S samples oxidized at 680°C:Solution A (left) vs. Solution B (right).

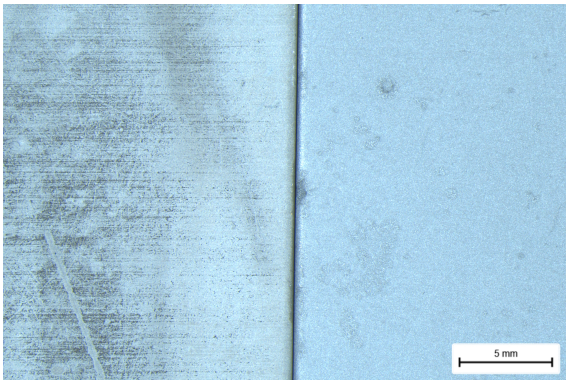


(d) Descaled 310S samples oxidized at 600°C: Solution A (left) vs. Solution B (right).

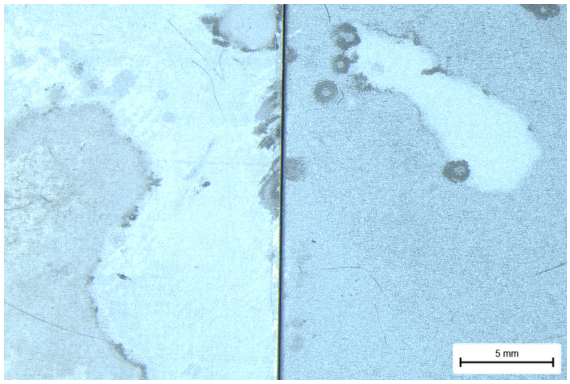
Figure 4.8: Stereoscopic images of 310S samples oxidized at different temperatures and descaled using both Solution A (left) vs. Solution B (right).



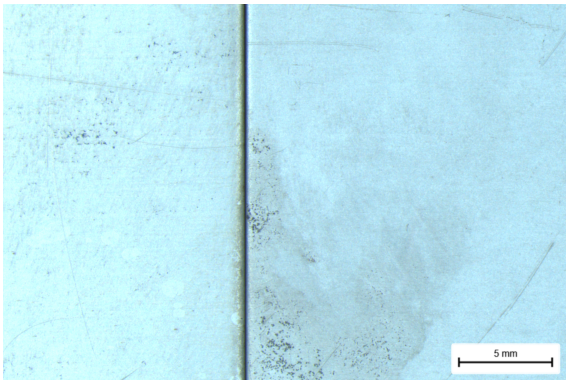
(a) Descaled 316L samples oxidized at 950°C: Solution A (left) vs. Solution B (right).



(b) Descaled 316L samples oxidized at 800°C: Solution A (left) vs. Solution B (right)

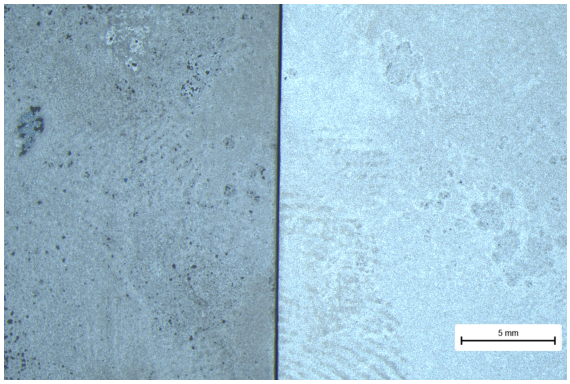


(c) Descaled 316L samples oxidized at 680°C: Solution A (left) vs. Solution B (right).

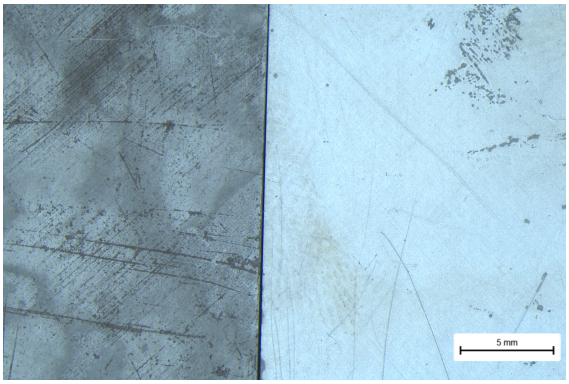


(d) Descaled 316L samples oxidized at 600°C: SSolution A (left) vs. Solution B (right).

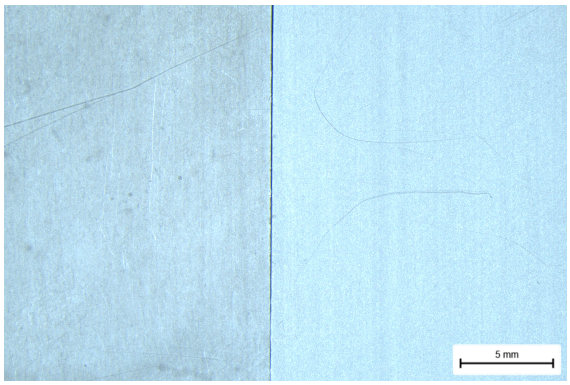
Figure 4.9: Stereoscopic images of 316L samples oxidized at different temperatures and descaled using both Solution A (left) vs. Solution B (right).



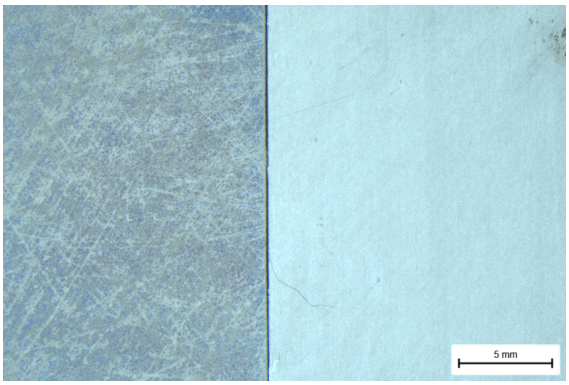
(a) Descaled 347 samples oxidized at 950°C: Solution A (left) vs. Solution B (right).



(b) Descaled 347 samples oxidized at 800°C: Solution A (left) vs. Solution B (right).



(c) Descaled 347 samples oxidized at 680°C: Solution A (left) vs. Solution B (right).



(d) Descaled 347 samples oxidized at 600°C: Solution A (left) vs. Solution B (right).

Figure 4.10: Stereoscopic images of 347 samples oxidized at different temperatures and descaled using both Solution A (left) vs. Solution B (right).

From the data collected Solution B was more efficient in term of descaling than solution A especially at higher oxidation temperature. However, even though Solution A was excluded from further use in Phase 2, as less effective and more time consuming, it remains a promising and less environmentally hazardous option. It could be considered in future studies aimed at developing more sustainable methods for descaling austenitic stainless steel.

In order to gain a better understanding of the process and its efficiency, such as its aggressiveness towards the base material and to observe the possible presence of oxide residues, intergranular corrosion, or cracks, it is necessary to examine the cross section of each sample using a optical microscope.

4.4 Optical microscope analysis

The optical microscope is an instrument that allows to observe specific elements impossible to see with naked eye [46]. In this report it was used to measure the extent of the oxide scale, assess the presence and the extent of cracks or intergranular corrosion and observe whether any oxide scale residues were left on the descale surface. The optical microscope used was a Leica DM6 M presents in the metal laboratory. The main challenge encountered with the optical microscope was related

to the thickness of the cross section. In fact, the thinner the sample the more difficult it was to obtain a flat cross section. Moreover, since the sample needed to be cut and subsequently mounted and polished, it is possible that some spallation occurred, resulting in the loss of a small amount of the oxide scale. For the same reasons explained previously, such as time constraint, only the cross sections of the four materials used in Phase 2 were analyzed.

In the following pages, the cross sections of the materials oxidized and descaled during Phase 1 will be compared in order to observed the difference in the oxide scale at different oxidizing temperatures, as well as the difference in the descaling methods at different oxidizing temperature.

4.4.1 Cross section AISI 304

The first material analyses with the optimal microscope was 304. As shown in Figure 4.12, 304 exhibits a uniform oxide scale. Below 800°C, the oxide scale is approximately 3-4 μm thick, while when the temperature increases to 950°C, the material shows signs of intergranular corrosion, penetrating as deep as about 8 μm, as displayed in Figure 4.12a. This is probably due to sensitization: even though 950°C is outside of the sensitization range for 304 stainless steel[19], as it is shown in Figure 4.11, during the heating process, the sample spent approximately three hours within the sensitization range. Since no annealing process was performed, the intergranular corrosion observed may result from this type of exposure. At 950°C, in fact, the interested area was already chromium depleted, making the material susceptible to corrosion at this temperature.

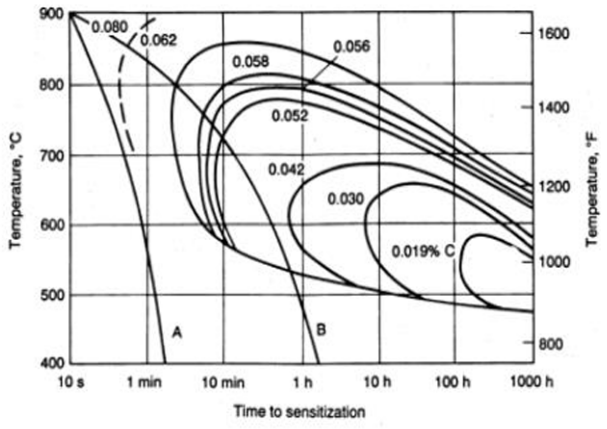
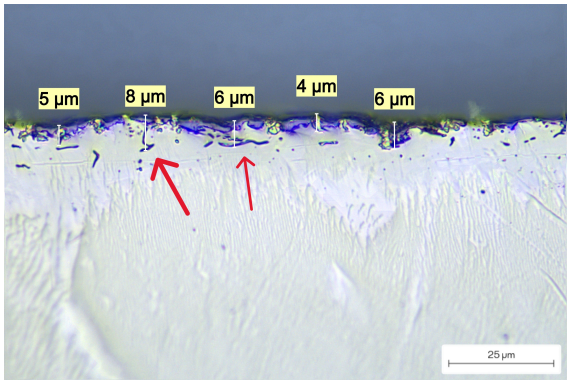
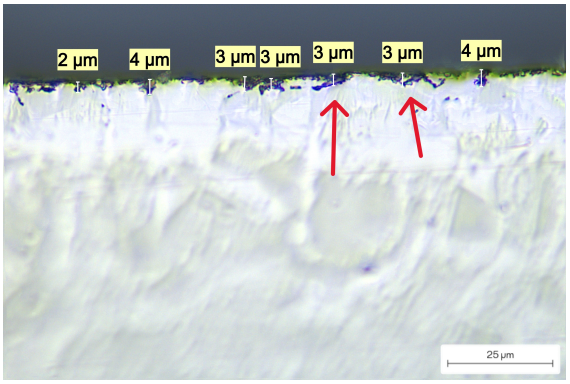


Figure 4.11: Time-Temperature Sensitization (TTS) for AISI 304 [47].

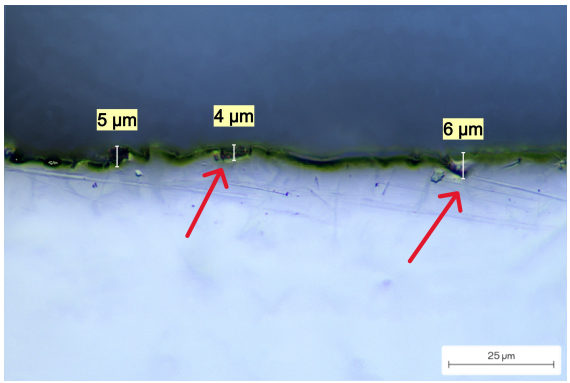
At 800 °C (fig. 4.12b), the intergranular corrosion is still present, though less extended than at 950°C, while at lower temperature tested, below 680°C, the surface appears slightly jagged. Due to the limited thickness of the oxide scale (approximately 1μm), the resolution of the optical microscope was a limiting factor, making observation and quantification of the oxide scale challenging.



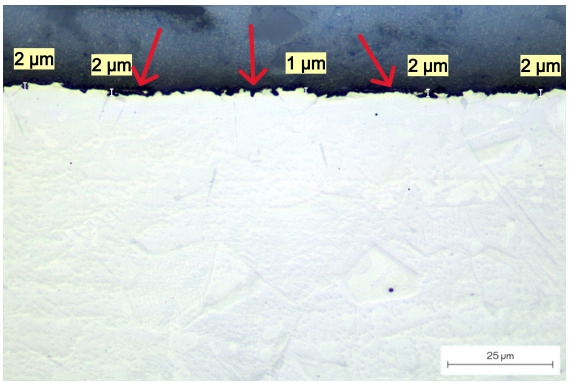
(a) Cross-section of the 304 sample oxidized at 950°C, showing evidence of intergranular corrosion, showing some jagged surface.



(b) Cross-section of the 304 sample oxidized at 800°C, showing evidence of intergranular corrosion.



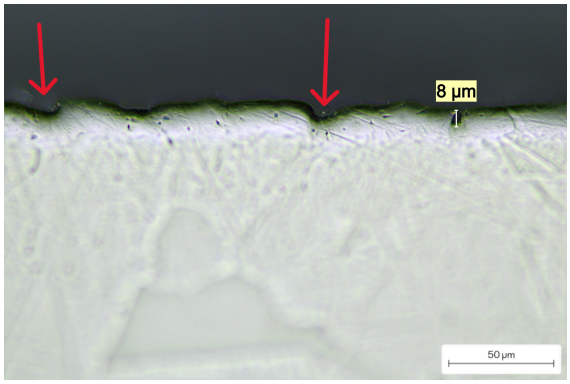
(c) Cross-section of the 304 sample oxidized at 680°C, showing a jagged oxide layer surface.



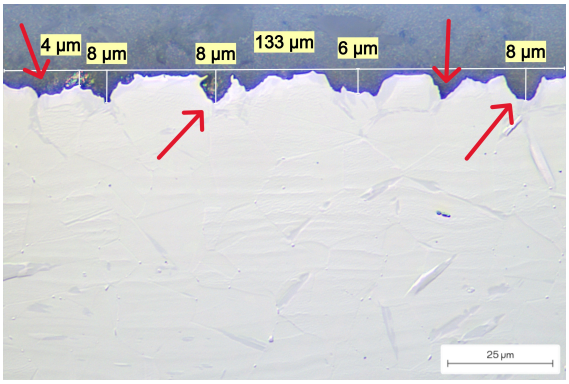
(d) Cross-section of the 304 sample oxidized at 600°C, showing a jagged oxide layer surface.

Figure 4.12: Optical microscope images of cross-sections of 304 samples oxidized at different temperatures.

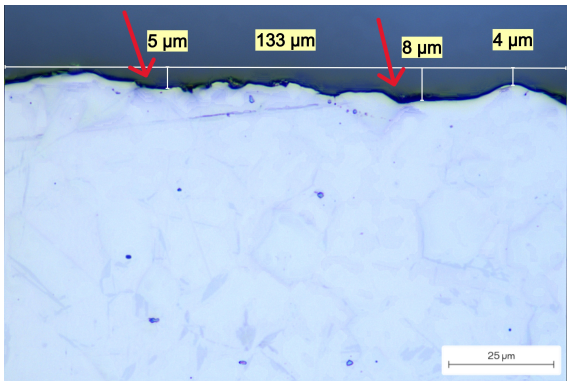
Figure 4.13 and Figure 4.14 show how material 304 reacted to exposure to Solution A and Solution B after being tested at different oxidizing temperatures. As both the descaled and oxidized samples underwent the same oxidizing cycle, all the samples were exposed to the sensitization range during the heating process. It is possible to observe in Figure 4.13 that the rock salt attacks cracks formed by intergranular corrosion and subsequently erodes part of the surface material: this phenomenon is especially noticeable at 800°C (Figure 4.13b). However, in case of Solution A, the affected depth is only a few microns, which does not appear problematic for the study's results.



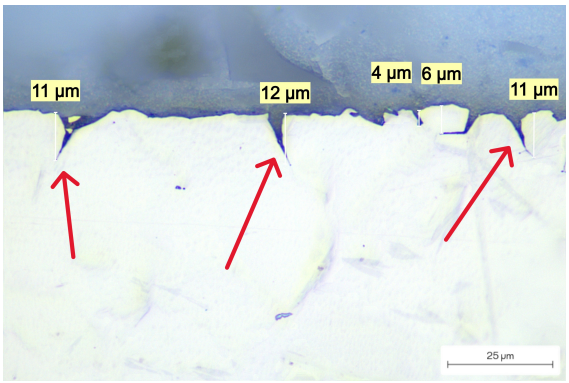
(a) Cross-section of the 304 sample oxidized at 950°C, and descaled with Solution A, showing slight surface erosion.



(b) Cross-section of the 304 sample oxidized at 800°Cand descaled with Solution A, showing surface erosion.



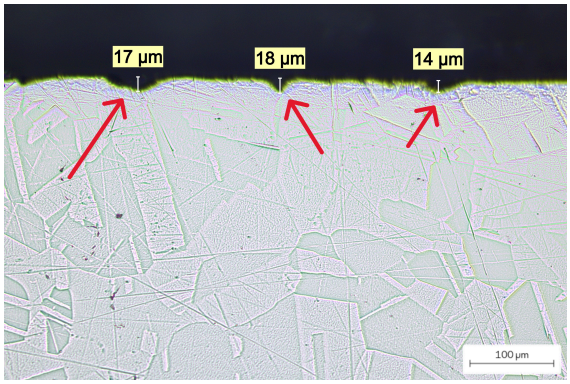
(c) Cross-section of the 304 sample oxidized at 680°C and descaled with Solution A, showing surface erosion.



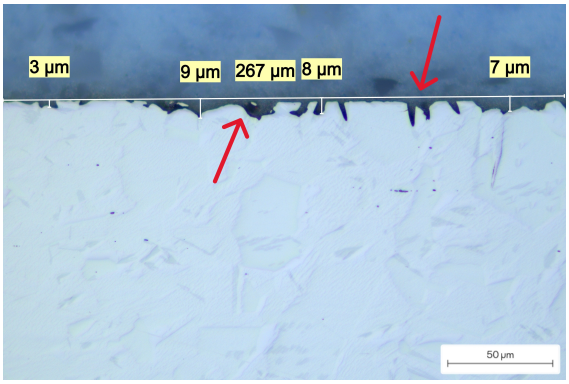
(d) Cross-section of the 304 sample oxidized at 600°Cand descaled with Solution A, showing surface erosion and intergranular corrosion.

Figure 4.13: Optical microscope images of cross-sections of 304 samples oxidized at different temperatures and descaled using Solution A.

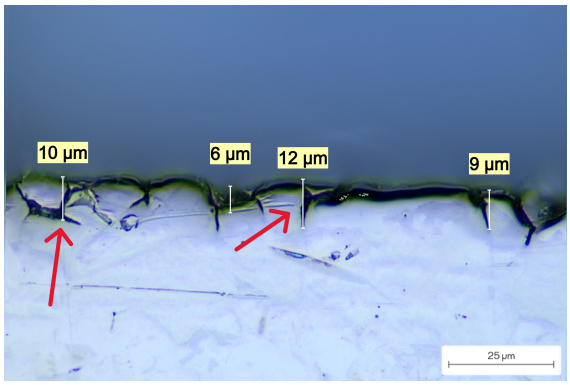
As shown in Figure 4.14, with Solution B, a similar phenomenon occurs as previously described with Solution A, but it is even more aggressive, as the acid responsible for removing the oxide scale is hydrofluoric acid. Especially at 600°C, as visible in the Figure 4.14d, it is evident that the hydrofluoric acid has penetrated into the base material, with intergranular corrosion observed up to 40μm or more (up to 52μm depending on the area). A depth of 40μm (or 52μm) does not represent a problem when considering the total area of the sample analyzed, making Solution B still the most effective option for this material. In fact, based on the sample dimensions, even though a larger portion of the sample is affected, for example, if 250μm along the base or height is considered, as the sample is rectangular, this only comprises between 3% and 13% of the total area, making the defect negligible for this application.



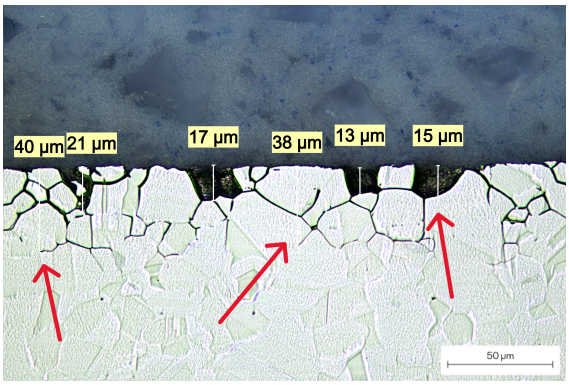
(a) Cross-section of the 304 sample oxidized at 950°C and descaled with Solution B, showing surface erosion.



(b) Cross-section of the 304 sample oxidized at 800°C and descaled with Solution B, showing surface erosion.



(c) Cross-section of the 304 sample oxidized at 680°C and descaled with Solution B, showing slight surface erosion and intergranular corrosion.



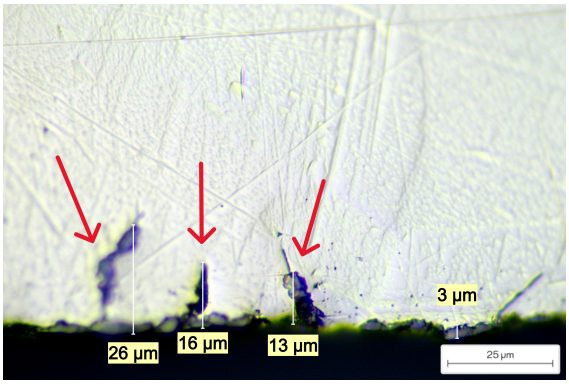
(d) Cross-section of the 304 sample oxidized at 600°C and descaled with Solution B, showing surface erosion and intergranular corrosion.

Figure 4.14: Optical microscope images of cross-sections of 304 samples oxidized at different temperatures and descaled using Solution B.

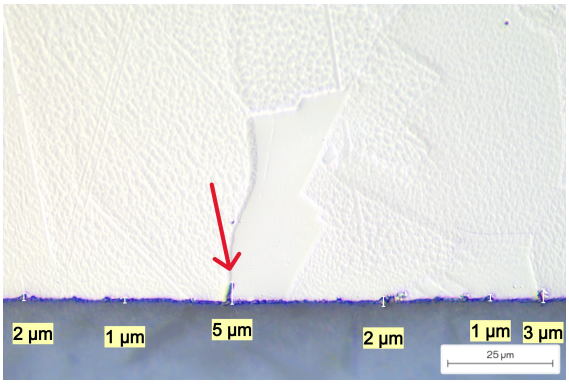
4.4.2 Cross section AISI 310S

The cross sections of the oxidized samples of 310S, presented in Figure 4.15, show different scenarios depending on the temperature. At 600°C (Figure 4.15d), the material exhibits a thin oxide scale (about 1μm or even less). While at 680°C and 800°C (Figure 4.15c and Figure 4.15b) the oxide scale appears slightly more inhomogeneous, ranging between the 1 and 5μm. At 950°C (Figure 4.15a), the most critical situation is observed, with several long cracks (ranging from 13μm and 26μm) and an uneven oxide scale layer.

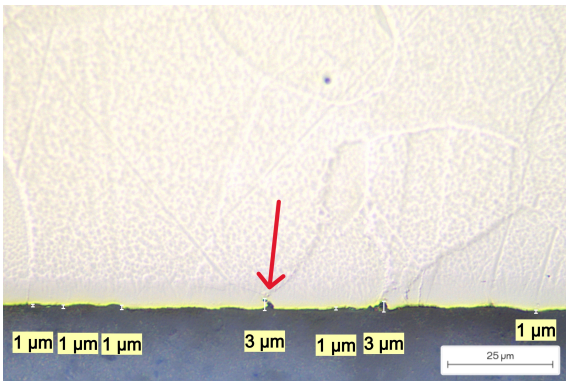
This cross sections are consistent with the data acquired and analyzed in the "mass gained" measurement section 4.2. According to the graph in Figure 4.2 and graph in Figure 4.3, 310S exhibits the lowest mass gained per area, at 600°C and a similarly low mass gained at 800°C. This correlates with the difficulty in observing the oxide scale even with the highest magnification of the optical microscope. Moreover, the presence of cracks aligns with the previously discussed behavior of sensitization, as all samples were loaded into and unloaded from the furnace simultaneously during both Phase 1.



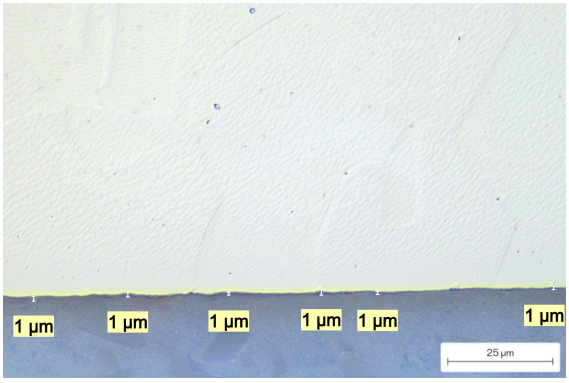
(a) Cross-section of the 310S sample oxidized at 950°C, showing intergranular corrosion.



(b) Cross-section of the 310S sample oxidized at 800°C, showing minor intergranular corrosion and a homogeneous oxide layer.



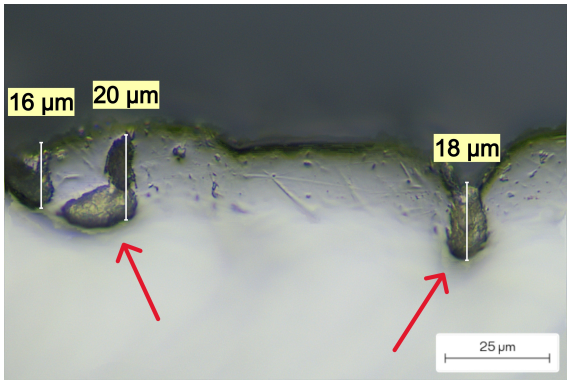
(c) Cross-section of the 310S sample oxidized at 680°C, showing minor intergranular corrosion and a homogeneous oxide layer.



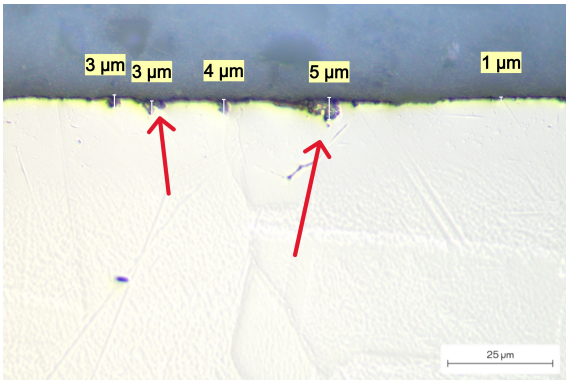
(d) Cross-section of the 310S sample oxidized at 600°C, showing a homogeneous oxide layer.

Figure 4.15: Optical microscope images of cross-sections of 310S samples oxidized at different temperatures.

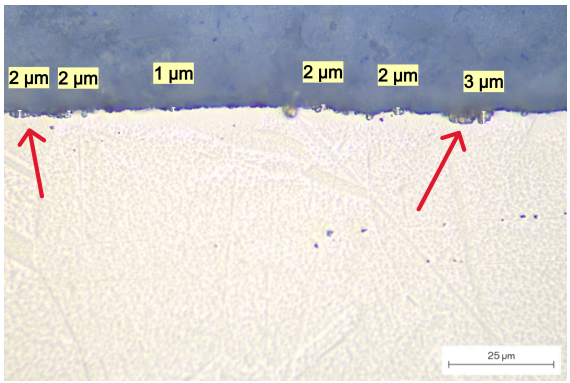
Solution A and Solution B exhibit different interaction with the oxidized 310S samples, as shown in Figure 4.16 and Figure 4.17. At the highest temperatures tested, specifically 950°C (Figure 4.16a) and 800°C (Figure 4.16b), the solution containing rock salt displayed the poorest results in terms of descaling efficacy. In fact, it is almost impossible to distinguish between the oxidized cross sections and those of the descaled samples. This behavior is likely not related to the nature of the oxide scale itself, as all the austenitic stainless steel form Cr_2O_3 when exposed to an oxidizing environment. Rather, is probably due to the high concentration of chromium and nickel present in the matrix, which create a substrate that is highly resistant to both high temperature corrosion and to descaling agents such as rock salt. At 680°C the sample descale with Solution A (Figure 4.16c) shows traces of erosion, approximately 7μm in depth. However, Solution A is effective only when the sample is exposed to 600°C, even though it is possible to observe some minor intergranular attacks on the base material.



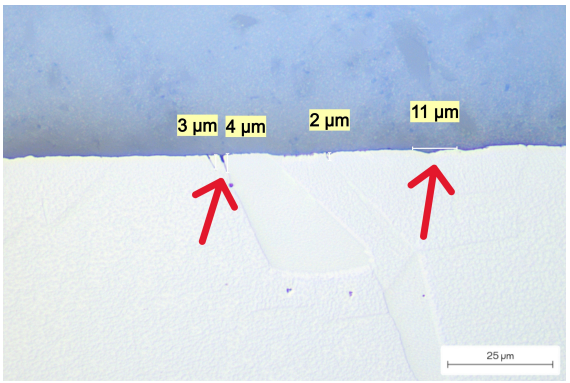
(a) Cross-section of the 310S sample oxidized at 950°C and descaled with Solution A, showing intergranular corrosion and residual oxide.



(b) Cross-section of the 310S sample oxidized at 800°C and descaled with Solution A, showing residual oxide.



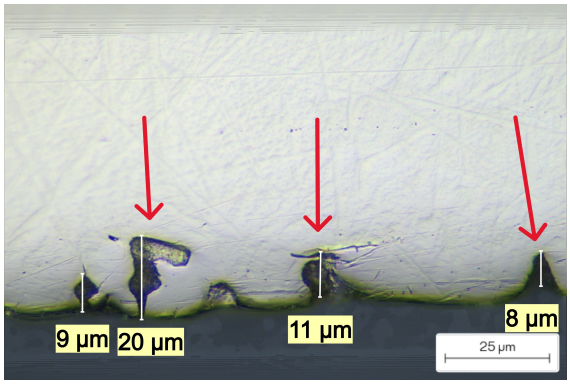
(c) Cross-section of the 310S sample oxidized at 680°C and descaled with Solution A, showing residual oxide.



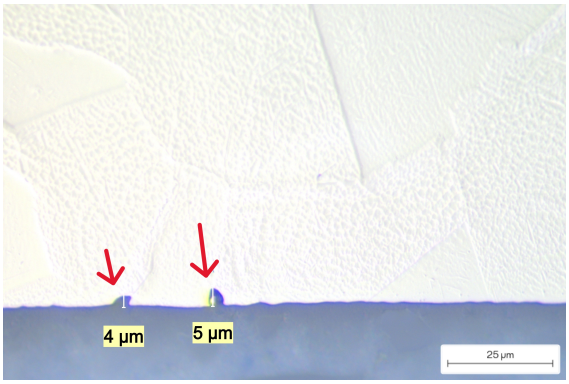
(d) Cross-section of the 310S sample oxidized at 600°C and descaled with Solution A, showing minor intergranular corrosion.

Figure 4.16: Optical microscope images of cross-sections of 310S samples oxidized at different temperatures and descaled using Solution A.

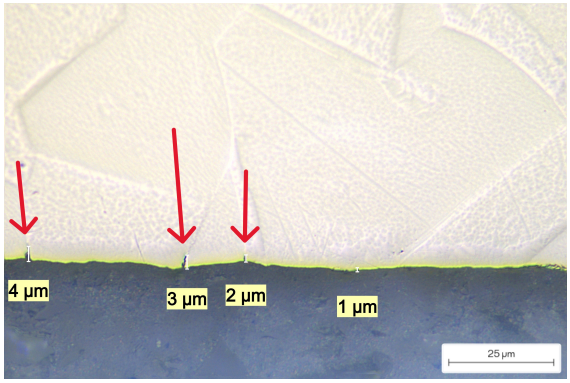
Solution B, on the other hand, exhibits good descaling results at almost every oxidizing temperature tested. Although the hydrofluoric acid presents in solution B is more effective, it tends to attack the grain boundaries, leading to accentuating the intergranular corrosion, especially at lower oxidizing temperature such as 600°C. This phenomenon is observed in all the sample exposed between 600°C and 800°C, with the extent of intergranular corrosion decreases as the oxidizing temperature increases. In fact, in Figure 4.17d, it is possible to observe an intergranular corrosion up to 18μm while at 800°C (Figure 4.17b), the maximum depth of intergranular corrosion decreases to 7μm. This is likely because, at lower oxidizing temperatures, a thinner oxide layer forms on the surface compared to higher temperature. For this reason, the descaling solution can penetrate easily after a 600°C cycle than a 800°C cycle.



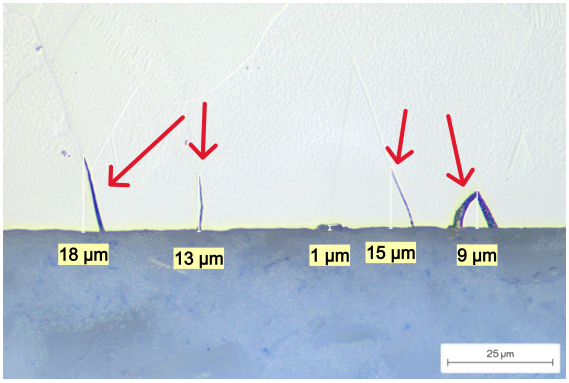
(a) Cross-section of the 310S sample oxidized at 950°C and descaled with Solution B, showing intergranular corrosion and residual oxide.



(b) Cross-section of the 310S sample oxidized at 800°C and descaled with Solution B, showing minor intergranular corrosion.



(c) Cross-section of the 310S sample oxidized at 680°C and descaled with Solution B, showing minor intergranular corrosion.

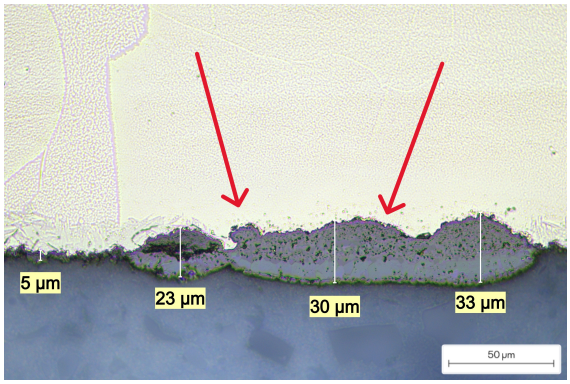


(d) Cross-section of the 310S sample oxidized at 600°C and descaled with Solution B, showing intergranular corrosion.

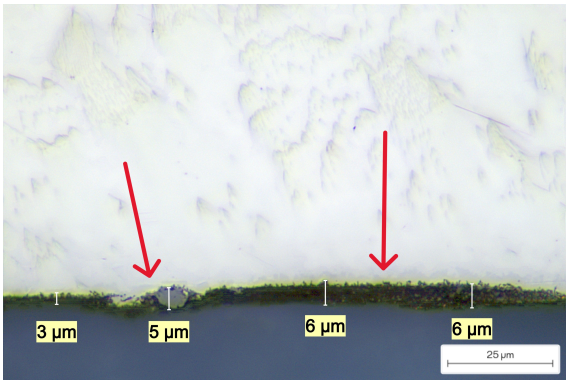
Figure 4.17: Optical microscope images of cross-sections of 310S samples oxidized at different temperatures and descaled using Solution B.

4.4.3 Cross section AISI 316L

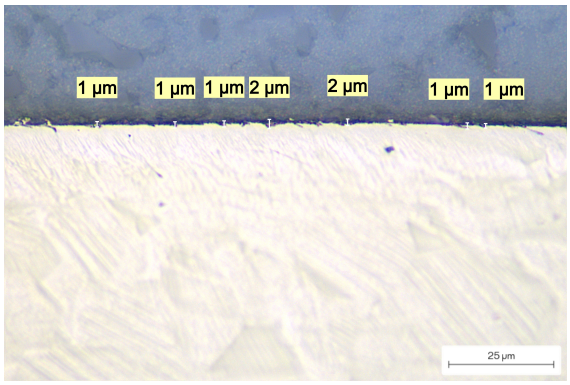
The third material analyzed through using the optical microscope was 316L. Figure 4.18 shows the cross section of its samples after the four oxidizing cycle at different temperatures, followed by descaling with the two different acids solutions. Among the material studied, 316L exhibit the poorest oxidation resistance at 950°C. This is due to its lower chromium content and the inability of molybdenum to protect the material at such high temperature [28]. As shown in Figure 4.18b, in addition to an oxide scale approximately 5μm thick, there are visible deposits of oxide scale ranging between 23μm to 33μm. It is possible that these deposits contain iron oxide, which is undesirable as it does not act as a protective layer. At 800°C, Figure 4.18b, the situation stabilizes: no prominent deposits are present, and a more homogeneous oxide layer between 3μm and 6μm is observed. Between 680°C (Figure 4.18c) and 600°C (4.18d), there is no significant difference in the oxide scale thickness, which in both cases is ranging between 1μm and 2μm. However, at higher temperature than 600°C, small areas of intergranular corrosion become visible.



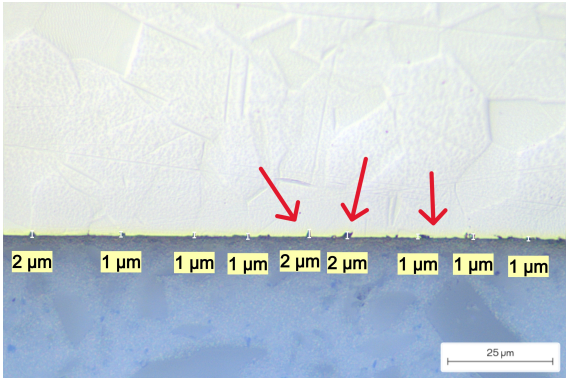
(a) Cross-section of the 316L sample oxidized at 950°C, showing an oxide chunk.



(b) Cross-section of the 316L sample oxidized at 800°C, showing a more homogeneous oxide scale.



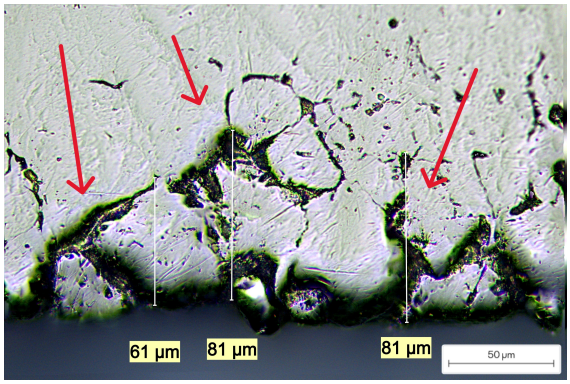
(c) Cross-section of the 316L sample oxidized at 680°C, showing a homogeneous oxide scale.



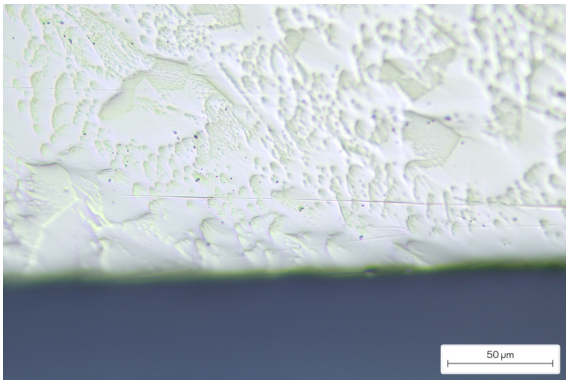
(d) Cross-section of the 316L sample oxidized at 600°C, showing a homogeneous oxide scale and minor intergranular corrosion.

Figure 4.18: Optical microscope images of cross-sections of 316L samples oxidized at different temperatures.

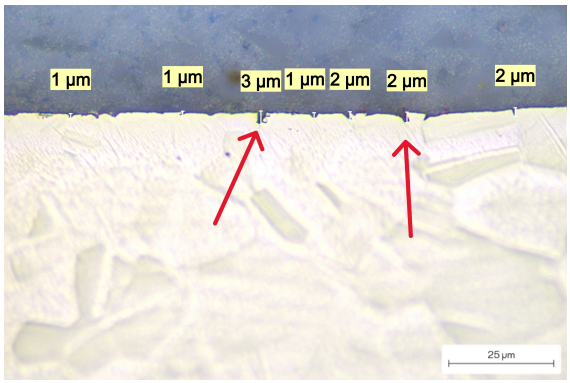
The cross section of the descaled sample for both Solution A and Solution B are shown in Figure 4.19 and Figure 4.20. Both solutions show promising results for the material 316L. At 950°C, Figure 4.19a, the rock salt erodes and attacks the intergranular corrosion already present after the oxidizing cycle, however, since 316L exhibits poor behavior at this temperature, the outcomes were not expected to be optimal. At 800°C, Figure 4.19b, the descaled performance is likely one of the most remarkable among the four temperatures and materials for Solution A, as no oxide scale is present and no intergranular corrosion appears to be observed. At 600°C, Figure 4.19d shows that the rock salt has eroded some of material's surface to a depth of approximately 13μm, and some intergranular corrosion is also visible. Another possible explanation for this observation is that the sample may not have been properly cut during the manual preparation, resulting in a small peak on the material's surface.



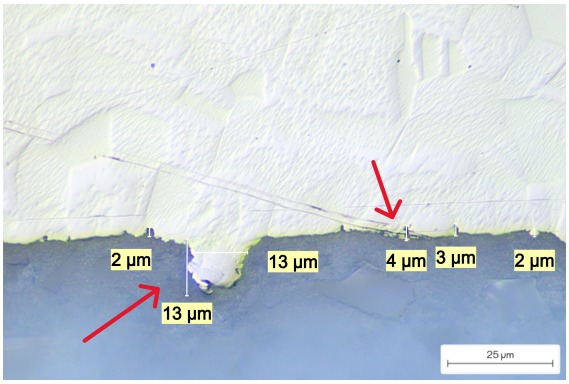
(a) Cross-section of the 316L sample oxidized at 950°C and descaled with Solution A, showing extensive intergranular corrosion.



(b) Cross-section of the 316L sample oxidized at 800°C and descaled with Solution A, showing a clean surface.



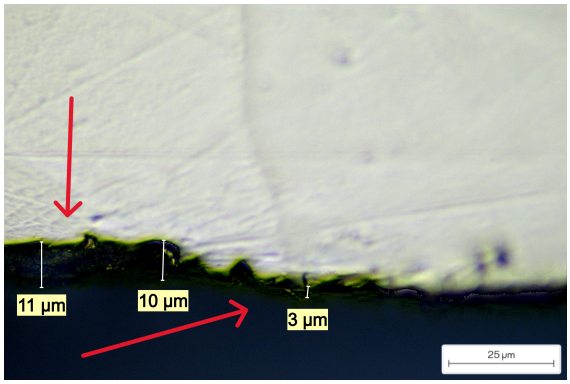
(c) Cross-section of the 316L sample oxidized at 680°C and descaled with Solution A, showing minor intergranular corrosion.



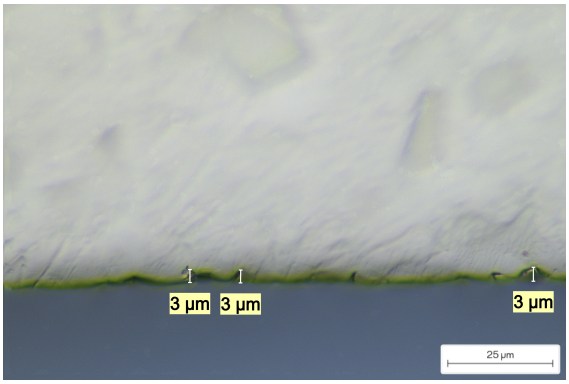
(d) Cross-section of the 316L sample oxidized at 600°C and descaled with Solution A, showing surface erosion and minor intergranular corrosion.

Figure 4.19: Optical microscope images of cross-sections of 316L samples oxidized at different temperatures and descaled with Solution A.

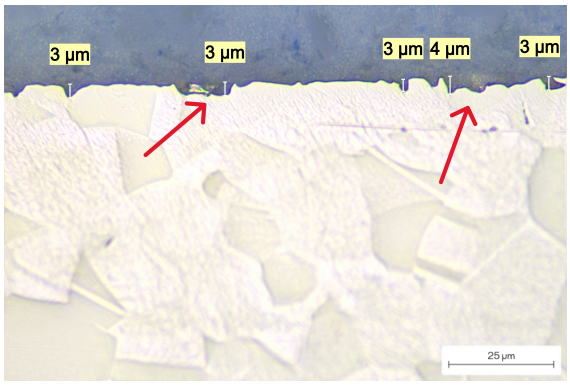
Solution B appears to display consistently positive results at all tested temperatures. At 950°C, Figure 4.20a, the oxide scale and some deposits are not completely removed, however the acid solution does not appear to have eroded the grain boundaries. At 800°C, Figure 4.20b, as with solution A, the surface appears clean and without any signs of intergranular corrosion. At 600°C, Figure 4.20d, some intergranular corrosion and voids are present, however they are negligible, as they range between 1μm and 2μm. The reason for the promising resistance shown to hydrofluoric acid solution can likely be attributed to the presence of molybdenum in the chemical composition. Molybdenum is known to increase the resistance under critical conditions, making the surface more resistant to this type of corrosive attack.



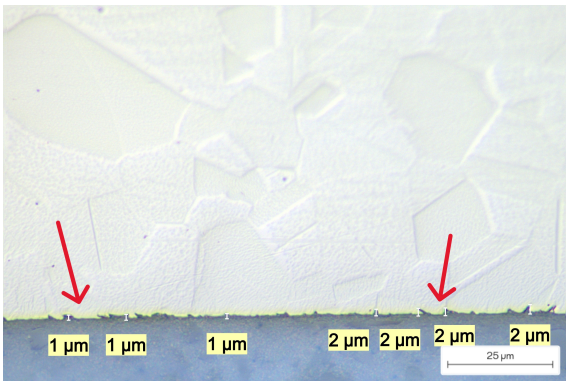
(a) Cross-section of the 316L sample oxidized at 950°C and descaled with Solution B, showing surface erosion and residual oxide.



(b) Cross-section of the 316L sample oxidized at 800°C and descaled with Solution B, showing minor intergranular corrosion.



(c) Cross-section of the 316L sample oxidized at 680°C and descaled with Solution B, showing minor surface erosion.

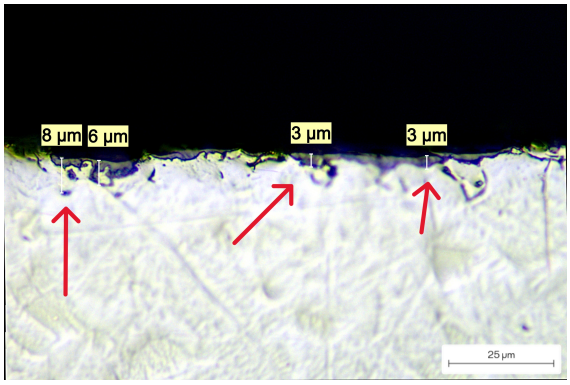


(d) Cross-section of the 316L sample oxidized at 600°C and descaled with Solution B, showing minor intergranular corrosion.

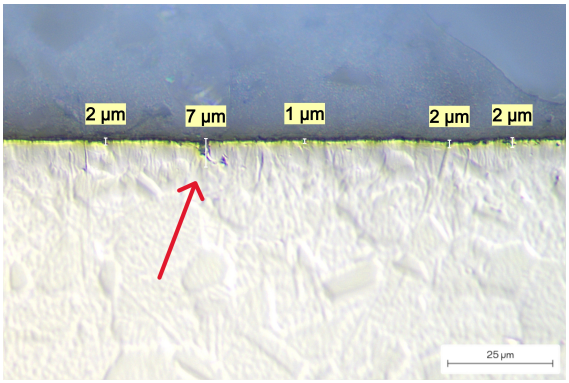
Figure 4.20: Optical microscope images of cross-sections of 316L samples oxidized at different temperatures and descaled with Solution B.

4.4.4 Cross section AISI 347

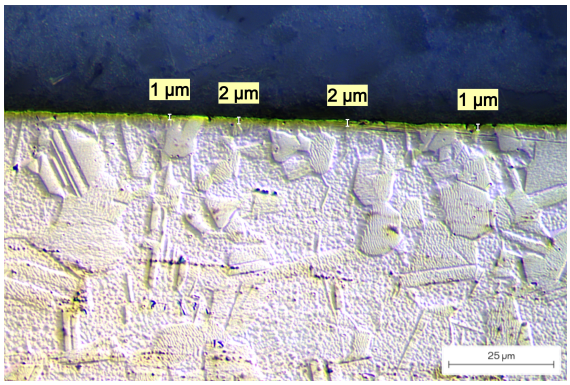
The cross sections of the different oxidized 347 samples are shown in Figure 4.21. Among the four austenitic stainless steel tested, 347 presented the most challenge for capturing the oxide layer using the high magnification microscope. As demonstrated by the mass gained per unit area in the Figure 4.2, 347 develops the lightest oxide scale layer. At the most critical temperature tested, 950°C (Figure 4.21a), it exhibits, in addition to some intergranular corrosion ranging between 6μm and 8μm, an oxide scale approximately 3μm thick. At 800°C (Figure 4.21b), the oxide scale is about 2μm thick and at 680°C and 600°C (Figure 4.21c and Figure 4.21d), it is almost 1μm or less. It is important to note that 347 is designed for aircraft applications. In addition to niobium, which helps reduce the carbide precipitation, it contains tantalum, making it highly corrosion resistant, especially in the range between 425°C to 815°C [48].



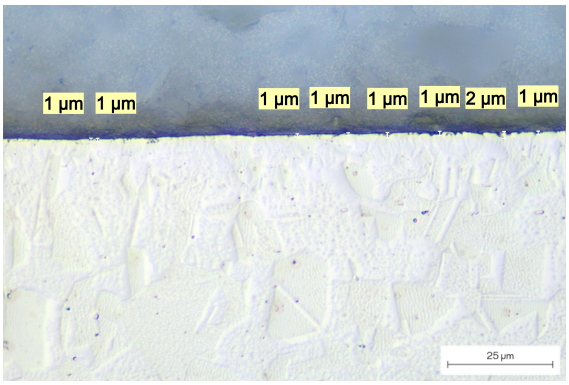
(a) Cross-section of the 347 sample oxidized at 950°C, showing intergranular corrosion.



(b) Cross-section of the 347 sample oxidized at 800°C, showing minor intergranular corrosion and a homogeneous oxide scale.



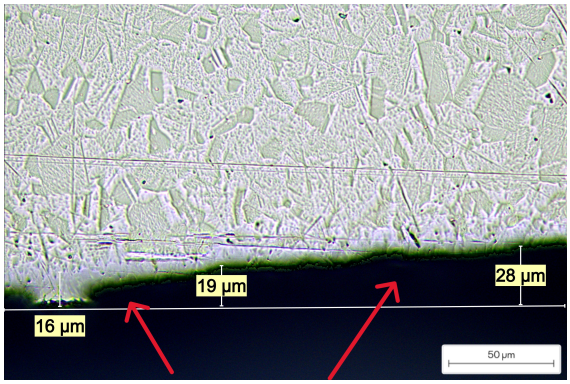
(c) Cross-section of the 347 sample oxidized at 680°C, showing a homogeneous oxide scale.



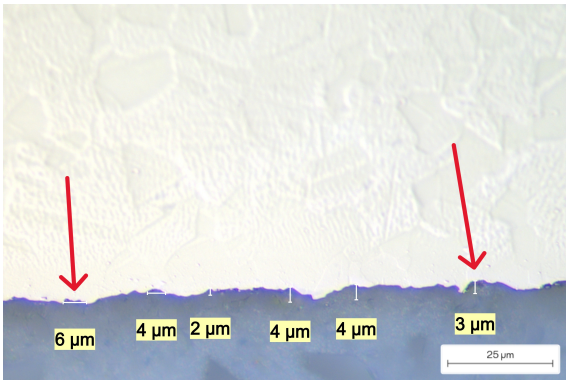
(d) Cross-section of the 347 sample oxidized at 600°C.

Figure 4.21: Optical microscope images of cross-sections of 347 samples oxidized at different temperatures.

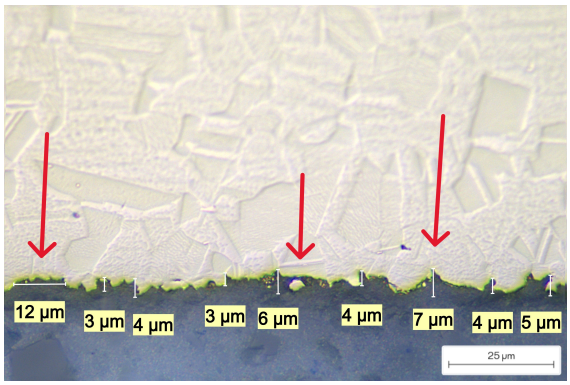
The cross sections of the samples that underwent the descaling process with Solution A and B are shown in Figure 4.22 and Figure 4.23. Solution A appears to erode portions of the material after all the oxidizing temperatures tested, ranging from 950°C to 600°C. Despite differences in temperature and the size of voids created (between 5μm and 28μm), the solution consistently causes material erosion in all scenarios, with greater severity observed at higher temperatures.
In comparison, Solution B appears less aggressive. In all the scenarios tested, a part at 680°C (Figure 4.23c), where the most significant intergranular corrosion and material erosion occurred, no voids or material erosion are present, unlike with Solution A.



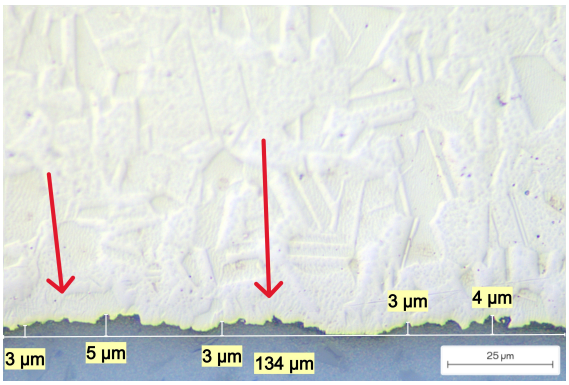
(a) Cross-section of the 347 sample oxidized at 950°C and descaled with Solution A, showing surface erosion.



(b) Cross-section of the 347 sample oxidized at 800°C and descaled with Solution A, showing surface erosion.

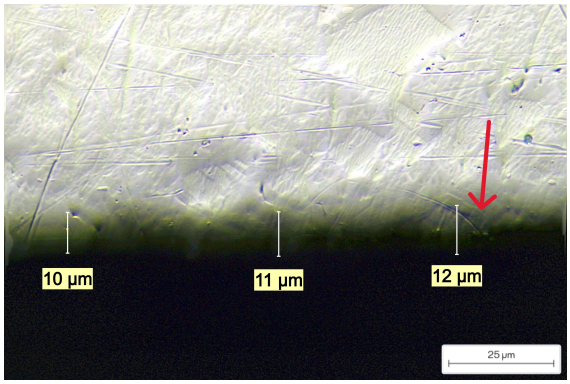


(c) Cross-section of the 347 sample oxidized at 680°C and descaled with Solution A, showing surface erosion.

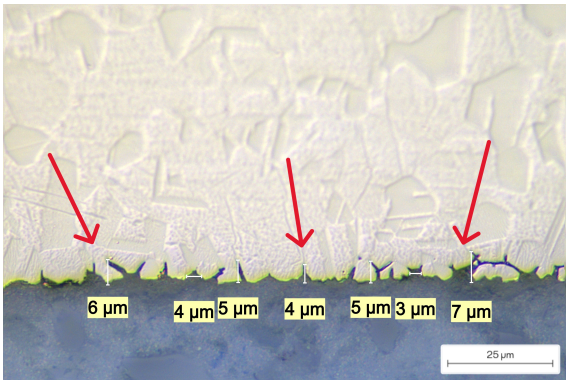


(d) Cross-section of the 347 sample oxidized at 600°C and descaled with Solution A, showing surface erosion.

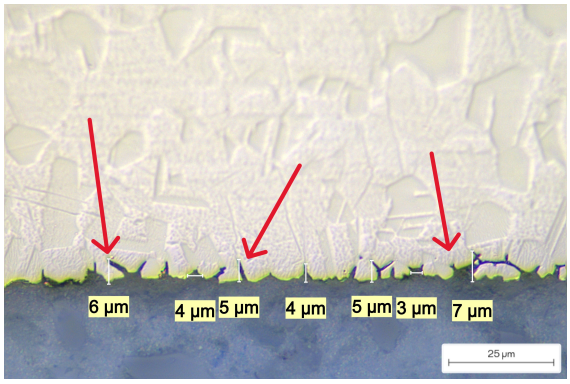
Figure 4.22: Optical microscope images of cross-sections of 347 samples oxidized at different temperatures and descaled using Solution A.



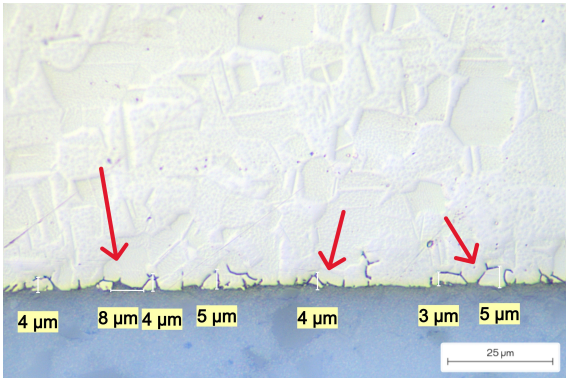
(a) Cross-section of the 347 sample oxidized at 950°C and descaled with Solution B, showing minor residual oxide.



(b) Cross-section of the 347 sample oxidized at 800°C and descaled with Solution B, showing minor surface erosion and minor intergranular corrosion.



(c) Cross-section of the 347 sample oxidized at 680°C and descaled with Solution B showing minor surface erosion and minor intergranular corrosion.



(d) Cross-section of the 347 sample oxidized at 600°C and descaled with Solution B, showing minor intergranular corrosion.

Figure 4.23: Optical microscope images of cross-sections of 347 samples oxidized at different temperatures and descaled using Solution B.

To summarize the observation from the optical microscope, the main factor influencing the material response to the oxidizing environment and to the descaling solutions is the chemical composition. 304, which has the simplest composition among the four austenitic stainless steels tested and is not enriched with any additional alloying elements, exhibits the poorest response to Solution B. In contrast, the other three materials, which contain either molybdenum, niobium or high chromium and nickel content, showed more promising results.

Moreover, the combination of low chromium concentration and the presence of molybdenum, as for 316L and the combination of low chromium and niobium, as for 347, enhances their resistance to intergranular corrosion, especially at lower temperature such as 600°C.
Solution A, which contains rock salt, appears to be more aggressive at lower temperature and increases the material erosion of these materials.
In conclusion, Solution A seems to be more effective for material with a simpler chemical composition or after the material has undergone a higher oxidizing temperature, such as 800°C. In contrast, for more complex chemical composition, the hydrofluoric acid solution, Solution B, appears to be

the better option in terms of descaling efficiency. It is important to note, however, that Solution B, while more effective based on the results, is more hazardous both environmentally and from a safety perspective.

4.5 Oxidation Kinetic Models

The oxidation kinetic model is the most effective method to represent the high temperature behavior of a material over time. As explained in the Literature review section 2.2, a material exposed to a high temperature oxidizing environment can exhibit a behavior that is typically approximated by one of these three models [33]:

1. Linear: $y = k \cdot t$
2. Parabolic: $y = k \cdot t^{0.5}$
3. Logarithmic: $y = k \cdot ln(t + 1)$

To determine which model best describes the behavior of the material under study, the experimental data points were used to optimize the parameter k for each equation. The value k was specific for every model and was selected to minimize the mean squared error, resulting in the best possible fit between the model and the collected data. Since the model obtained represents thickness loss over time, it was theorized that the material removed after descaling the sample provided an accurate approximation of long-term behavior of the material under oxidizing conditions at a certain temperature. As a result, material loss could be approximated by one of the oxidation kinetic models. The material loss over time models, represented by the lines, and the data collected, shown as points, are shown for 800°C and 600°C in Figure 4.24 and Figure 4.25.

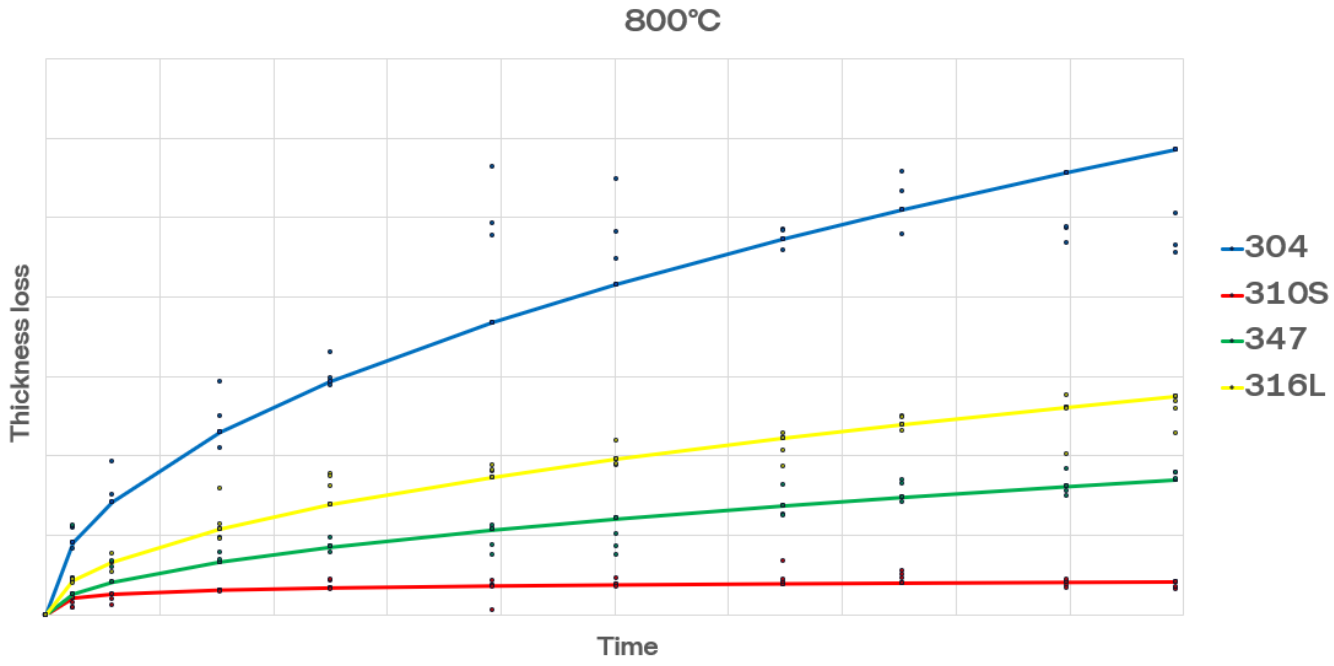


Figure 4.24: Thickness loss over time - oxidation temperature 800 °C.

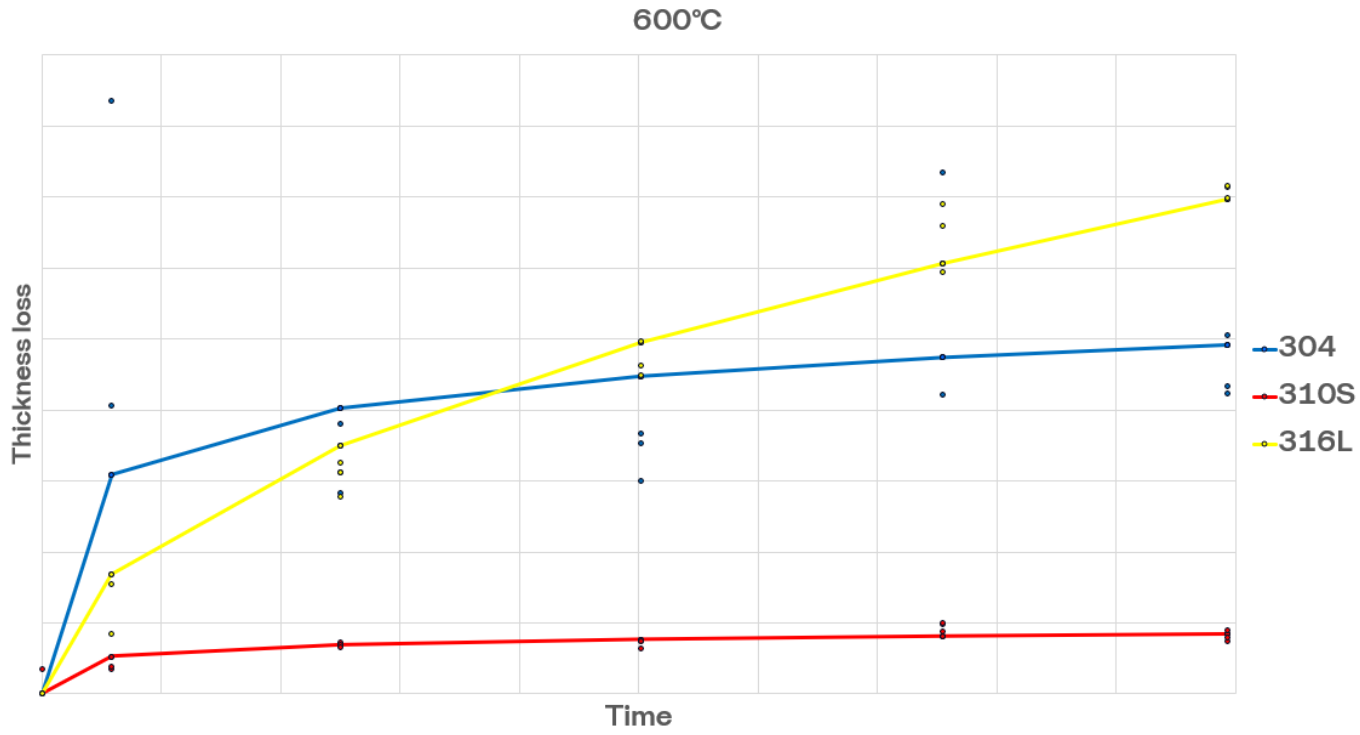


Figure 4.25: Thickness loss over time - oxidation temperature 600 °C.

As these graphs illustrate, temperature is a major factor influencing material performance in an oxidizing environment. At 800°C, the material that exhibits the greatest thickness loss over time is 304. This observation aligns with its previously recorded highest mass gained per unit area, confirming that 304 performs the worst among the austenitic stainless steel tested at this high temperature. In contrast, 304 appears to be more suitable for used at lower temperatures, such as 600°C, where it demonstrates a logarithmic behavior as opposed to the previously observed parabolic. Logarithmic behavior is the most optimal model a material can follow, as material loss over time will be lower compared to parabolic or linear trends.

316L is the material that, based on the collected data, performed the worst overall. Specifically, it exhibits the highest thickness loss over time at 600°C, and while at 800°C its thickness loss is not as significant as that of 304, in both scenarios it exhibits a parabolic behavior. Particularly at 600°C, this leads to significant material loss over time, considering that lower temperature are generally associated with longer expected lifetime. This likely indicated that 316L would perform better, in terms of material loss, at even lower temperatures than the one considered in this study.

Among all materials, 310S demonstrates the best performance at both oxidizing temperatures, exhibiting the lowest material loss in both scenarios and a logarithmic behavior over time. Even at 800°C, it maintains a logarithmic trend, suggesting that it could potentially perform well even at higher temperature. The same can be said for 347, which, due to spatial constraints of the Eff furnace, could only be tested at 800°C. However, it displayed good performance under these conditions, also exhibiting a logarithmic behavior, making it plausible that it would also be a good choice both at lower and higher temperatures, than the one tested as well.

To summarize, 310S and 347 exhibit the best performance in term of material loss, suggesting that

they could resist and perform well even at higher temperatures. In contrast 304 shows significant material loss at 800°C, while it stabilizes at 600°C. 316L, on the other hand, demonstrates the worst overall performance, especially at 600°C. Moreover, it was possible to identify a correlation between the mass gained over area and the oxidation kinetic model. In fact, even though the models followed by the materials in gaining and losing mass do not always remain consistent, it is possible to observe similarities when comparing the graphs. Specifically, the materials show similar tendencies in their mass gain per unit area over time and thickness loss over time. 304 and 316L exhibited the highest mass gained per area over time at 800°C and 600°C, respectively. As a result, these materials also experienced the greatest thickness loss over time at their respective oxidation temperatures. The same can be noticed for 310S and 347, which exhibited the lowest mass gained per unit area over time and showed the least thickness loss over time. These correlations suggest that materials which tend to gained more oxide scale also suffer greater material degradation under these specific conditions.

Chapter 5

Conclusion

In this thesis, different aspects of high temperature oxidation and the subsequent descaling process were studied. First, two descaling solutions were tested at room temperature. A group of six different austenitic stainless steel, each oxidized at four different temperatures, was descaled with both solutions. The most suitable descaling method was developed based on tests. The samples were then examined using both a stereoscopic and a optical microscopy to characterize the extent of the oxidate layer and to observe the effects of the two solutions, both on the surface and through cross sections. The solution containing hydrofluoric acid, Solution B, produced the best results compared to the one containing rock salt, Solution A. Solution A was more time-consuming and it was observed to attack the base material more aggressively, especially at 600°C, except for 304. However, Solution A showed some promising results with 304, and since it is less environmentally hazardous than Solution B, it could be worth researching further.

After this initial phase, four of the original six materials: 304, 310S, 316L and 347, were selected to study both their mass gained and their thickness loss over time at two temperatures: 800°C and 600°C. The samples were placed in the furnaces for a total of almost 2000 hours (nearly three months) and they were periodically removed for descaling every 10 or 20 days. This data allowed the development of comprehensive oxidation and thickness loss models over time.

From the data acquired, 310S was the best performing material both because it followed a logarithmic curve and had the lowest thickness loss at both temperatures. This is consistent with its chemical composition, as it contains the highest level of chromium and nickel. The second best material identified was 347, which is enriched with niobium and tantalum. This material developed a very thin oxide layer at almost every temperatures tested and also shows a logarithmic curve at 800°C making it a good alternative to 310S. 316L overall was the material with the worst response at both temperatures, despite the addition of molybdenum in its composition, its low chromium content prevent it from performing well at these temperatures. 304, despite showing the worst corrosion behavior at 800°C by losing the most material, showed promising results at 600°C.

In conclusion, the chemical composition of the alloys, combined with the oxidation temperature, represent the most influential factor in high temperature oxidation and the study of the thickness loss.

Chapter 6

Future work

The saturation point of both descaling solutions could be studied to determine how long they can be reused effectively. Another aspect not considered in this thesis is performing XRD analysis on the descaled samples, which would allow for quantifying the descaling process and evaluating the efficiency of the solutions beyond visual analysis. This report focused in a small group of materials, but the study could be expanded to include different stainless steels to predict their thickness loss over time in oxidizing environments.
Additionally, the chromium-depleted layer of the oxidized samples could be analyzed using EDSB to gain further insight into the oxidation process.

Bibliography

[1] British Stainless Steel Association. *High temperature corrosion*. https://bssa.org.uk/technical-help/corrosion/high-temperature-corrosion/. Accessed: 2026-04-29.

[2] B. Gleeson. *Thermodynamics and theory of external and internal oxidation of alloys*. https://www.researchgate.net/profile/BrianGleeson/publication/286545911_Thermodynamics_and_Theory_of_External_and_Internal_Oxidation_of_Alloys/links/56958a7b08ae425c68984f6f/Thermodynamics-and-Theory-of-External-and-Internal-Oxidation-of-Alloys.pdf. Retrieved 23/02/2026. 2015.

[3] M. Balachandar and M. Vinoth Kumar. "Hot corrosion behaviour of Super 304HCu austenitic stainless steel exposed to salt mixture at 900°C". In: *Journal of Materials Engineering and Performance* (2025). Advance online publication. URL: https://doi.org/10.1007/s11665-025-12676-3.

[4] B. N. Popov. "High-temperature corrosion". In: *Corrosion Engineering*. Ed. by B. N. Popov. Elsevier, 2015, pp. 481–523. URL: https://doi.org/10.1016/B978-0-444-62722-3.00011-2.

[5] B. Amjadian. *Advanced descaling techniques for high-temperature oxidation in stainless-steel alloys (Student paper)*. https://lup.lub.lu.se/student-papers/record/9198823. Lund University Student Papers. 2025.

[6] S. Prakash. "7 - Hot corrosion of alloys and coatings". In: *Developments in high temperature corrosion and protection of materials*. Ed. by W. Gao and Z. Li. Woodhead Publishing, 2008, pp. 164–191. URL: https://doi.org/10.1533/9781845694258.1.164.

[7] Y. Shinata, F. Takahashi, and K. Hashiura. "NaCl-induced hot corrosion of stainless steels". In: *Materials Science and Engineering* 87 (1987), pp. 399–405. DOI: 10.1016/0025-5416(87)90404-6. URL: https://doi.org/10.1016/0025-5416(87)90404-6.

[8] Discovery Alert. *Stainless steel market 2025: Dynamics, prices, costs*. https://discoveryalert.com.au/stainless-steel-market-2025-dynamics-prices-costs/. Retrieved 25/02/2026. 2024.

[9] Wikipedia. *Nickel pig iron*. https://en.wikipedia.org/wiki/Nickel_pig_iron. In Wikipedia. Retrieved 25/02/2026.

[10] MARC Group. *Stainless steel pricing report*. https://www.imarcgroup.com/stainless-steel-pricing-report. Retrieved 25/02/2026.

[11] Specialty Steel Industry of North America (SSINA). *Descaling Stainless Steel*. Retrieved 26/03/2026. 2026. URL: https://www.ssina.com/education/fabrication/descaling-stainless-steel/.

[12] G. W. Meetham and M. H. Voorde. *Materials for High Temperature Engineering Applications*. Springer-Verlag Berlin Heidelberg, 2000. DOI: 10.1007/978-3-642-56938-8. URL: https://doi.org/10.1007/978-3-642-56938-8.

[13] Alessio Malandruccolo. *Superaustenitic Stainless Steels: A Comprehensive Overview*. Springer, 2024. DOI: 10.1007/978-3-031-68744-0. URL: https://doi.org/10.1007/978-3-031-68744-0.

[14] S. Gialanella and A. Malandruccolo. "Aerospace Alloys". In: *Aerospace Alloys*. Chapter 5. Springer, 2020. DOI: 10.1007/978-3-030-24440-8. URL: https://doi.org/10.1007/978-3-030-24440-8.

[15] Encyclopædia Britannica. *Stainless Steel*. In Encyclopædia Britannica. Retrieved 25/02/2026. 2026. URL: https://www.britannica.com/technology/stainless-steel.

[16] R. M. Davidson, T. DeBold, and M. J. Johnson. "Corrosion of Stainless Steels". In: *ASM Handbook, Volume 13: Corrosion*. Ed. by S. D. Cramer and Jr. Covino B. S. 4th printing. ASM International, 1987, pp. 547–565.

[17] Joe. *The Science of Passivation: Understanding How Chromium and Nickel Protect Stainless Steel Enclosures*. VIOX Electric. Retrieved 2026-04-29. Jan. 30, 2026. URL: https://viox.com/science-of-passivation-stainless-steel-enclosures/.

[18] A. Paúl et al. "The Role of Silicon in the Reactive-Elements Effect on the Oxidation of Conventional Austenitic Stainless Steel". In: *Oxidation of Metals* 67.1 (2007), pp. 87–105. DOI: 10.1007/s11085-006-9046-6. URL: https://doi.org/10.1007/s11085-006-9046-6.

[19] "Glossary of Terms". In: *ASM Handbook, Volume 13: Corrosion*. Ed. by S. D. Cramer and Jr. Covino B. S. 4th printing. ASM International, 1987, p. 11.

[20] S. L. Pohlman. "General Corrosion". In: *ASM Handbook, Volume 13: Corrosion*. Ed. by S. D. Cramer and Jr. Covino B. S. 4th printing. ASM International, 1987, pp. 80–103.

[21] King S.p.A. *AISI 304: Characteristics, Applications and Comparison with Other Stainless Steels*. King Inox. Retrieved 26/03/2026. 2026. URL: https://king-inox.com/en/aisi-304-characteristics-applications/.

[22] SAKY Steel. *What are the Common Applications of Grade 310/310S Stainless Steel?* Retrieved 26/03/2026. 2026. URL: https://www.sakysteel.com/news/what-are-the-common-applications-of-grade-310310s-stainless-steel.

[23] Steel Pro Group. *Grade 347 Stainless Steel*. Retrieved 26/03/2026. 2026. URL: https://steelprogroup.com/stainless-steel/grades/grade-347/.

[24] Metal Zenith. *253MA Stainless Steel: Properties and Key Applications*. Retrieved 26/03/2026. 2026. URL: https://metalzenith.com/blogs/steel-properties/253ma-stainless-steel-properties-and-key-applications.

[25] Jacquet USA. *Technical Sheet A800H/800HT*. Aug. 2025. URL: https://usa.myjacquet.com/wp-content/uploads/sites/55/2025/08/Technical_Sheet_A800H_800HT.pdf.

[26] MatWeb. *304 stainless steel*. Retrieved 2026-03-26. 2026. URL: https://www.matweb.com/search/DataSheet.aspx?MatGUID=abc4415b0f8b490387e3c922237098da.

[27] MatWeb. *AISI Type 310S stainless steel, annealed*. Retrieved 2026-03-26. n.d. URL: https://www.matweb.com/search/DataSheet.aspx?MatGUID=9d42d23b1d2e4afc8912f32f1d1e63b6.

[28] MatWeb. *316L stainless steel, annealed plate*. Retrieved 2026-03-26. 2026. URL: https://www.matweb.com/search/DataSheet.aspx?MatGUID=530144e2752b47709a58ca8fe0849969.

[29] MatWeb. *347 stainless steel, annealed, sheet*. Retrieved 2026-03-26. 2026. URL: https://www.matweb.com/search/DataSheet.aspx?MatGUID=674116a5648146d2b1916a84599e4dd6.

[30] Alleima. *Alleima® 253 MA Tube and pipe, seamless Datasheet [PDF]*. Retrieved 2026-03-26. May 2025. URL: https://www.alleima.com/en/technical-center/material-datasheets/tube-and-pipe-seamless/alleima-253-ma/?show=pdf.

[31] Corrosion Materials. *Alloy 800 Technical Data Sheet*. Retrieved 2026-03-26. 2026. URL: https://corrosionmaterials.com/wp-content/uploads/docs/Alloy800.pdf.

[32] N. Perez. *Electrochemistry and Corrosion Science*. 2nd ed. Springer, 2016. DOI: 10.1007/978-3-319-24847-9. URL: https://doi.org/10.1007/978-3-319-24847-9.

[33] A. S. Khanna. "High-temperature oxidation". In: *Handbook of Environmental Degradation of Materials*. Ed. by M. Kutz. 3rd ed. William Andrew Publishing, 2018, pp. 117–132. DOI: 10.1016/B978-0-323-52472-8.00006-X. URL: https://doi.org/10.1016/B978-0-323-52472-8.00006-X.

[34] E. McCafferty. *Introduction to Corrosion Science*. Springer, 2010. DOI: 10.1007/978-1-4419-0455-3. URL: https://doi.org/10.1007/978-1-4419-0455-3.

[35] J. Bai, H. Li, and G. Wang. "Review on evolution of oxide layer and chromium depletion layer of austenitic stainless steel during industrial processing". In: *Steel Research International* 96.10 (2025), pp. 13–32. URL: https://doi.org/10.1002/srin.202400938.

[36] Y. Yin et al. "Grain boundary chromium depletion in austenitic alloys". In: *Journal of Materials Science* 45.21 (2010), pp. 5872–5882. DOI: 10.1007/s10853-010-4666-2. URL: https://doi.org/10.1007/s10853-010-4666-2.

[37] MachineMfg. *How to descale stainless steel: An overview*. Retrieved 2026-03-26. 2026. URL: https://shop.machinemfg.com/how-to-descale-stainless-steel-an-overview/.

[38] Steel Pro Group. *Passivated stainless steel finish*. Retrieved 2026-03-26. 2026. URL: https://steelprogroup.com/stainless-steel/finish/passivated/.

[39] M. Maanonen. "Steel pickling in challenging conditions". Theseus. Bachelor's thesis. Saimaa University of Applied Sciences, 2014. URL: https://www.theseus.fi/bitstream/handle/10024/70713/Steel_Pickling_in_Challenging_Conditions_2014_Thesis_Mika_Maanonen.pdf?sequence=1.

[40] W. Homjabok, S. Permpoon, and G. Lothongkum. "Pickling behavior of AISI 304 stainless steel in sulfuric and hydrochloric acid solutions". In: *Journal of Metals, Materials and Minerals* 20.2 (2010). Article 1. URL: https://digital.car.chula.ac.th/jmmm/vol20/iss2/1.

[41] ASTM International. *Standard practice for cleaning, descaling, and passivation of stainless steel parts, equipment, and systems (ASTM A380/A380M 17)*. https://www.astm.org/a0380_a0380m-17.html. 2017.

[42] P. Gillström and M. Jarl. "Mechanical descaling of wire rod using reverse bending and brushing". In: *Journal of Materials Processing Technology* 172.3 (2006), pp. 332–340. DOI: 10.1016/j.jmatprotec.2005.10.014. URL: https://doi.org/10.1016/j.jmatprotec.2005.10.014.

[43] A. Dutta and R. McCracken. "Microstructural aspects of the corrosion of Alloy 800". In: *Corrosion Science* 46.12 (2004), pp. 2937–2953. DOI: 10.1016/j.corsci.2004.04.005.

[44] J. Pires and A. A. Makinde. "High temperature oxidation: Stainless-steel alloys". Lund University Student Papers. Master's thesis. Lund University, Production and Materials Engineering, 2024. URL: http://lup.lub.lu.se/student-papers/record/9158258.

[45] Leica Microsystems. *M125 C, M205 C & M205 A Encoded stereo microscopes*. Accessed: 2026-05-22. 2026. URL: https://www.leica-microsystems.com/products/light-microscopes/stereo-microscopes/p/leica-m125-c/.

[46] George Youssef. "Characterization of polymers". In: *Applied Mechanics of Polymers*. Elsevier, 2022, pp. 273–299. ISBN: 978-0-12-821078-9. DOI: 10.1016/B978-0-12-821078-9.00016-8. URL: https://www.sciencedirect.com/science/article/pii/B9780128210789000168.

[47] Reena Nagar, Krunal Patel, and Kaizar Bhaisaheb. "A review: Sensitization in stainless steel". In: *International Research Journal of Modernization in Engineering Technology and Science* 6.1 (Jan. 2024). Impact Factor: 7.868. DOI: 10.56726/IRJMETS48865. URL: https://www.irjmets.com.

[48] Metallica Metals. *Datasheet for Stainless Steel 347/347H*. https://www.steelpipesfactory.com/wp-content/uploads/2021/05/Datasheet-For-Stainless-Steel-347-347H.pdf. Steel Pipes Factory. 2021.